Original Article | **Open Access**

Extracellular Vesicles and Circulating Nucleic Acids

Vardanyan *et al. Extracell Vesicles Circ Nucleic Acids.* 2026;7:1751-74 **DOI:**10.20517/evcna.2026.91

Temozolomide reshapes concentration, morphology, proteome, and biological activity of glioblastoma-derived extracellular vesicles

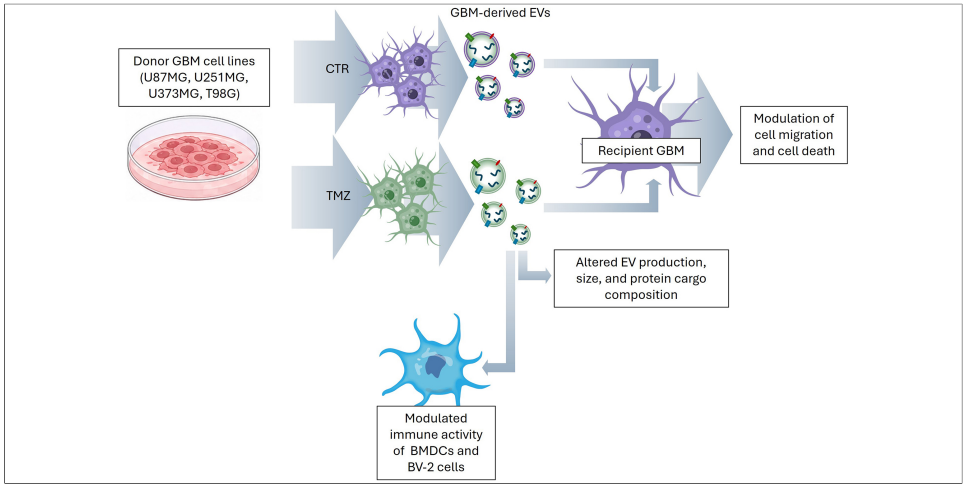
Diana Vardanyan[1,#], Mariana Karimova[2,#], Iulia Efimova[2,3], Federica Fratini[4], Simone Dinarelli[5], Maria Concetta Cufaro[6,7], Marcello Chieppa[8], Maurizio Zuccotti[9], Andrea Alfieri[10], Piero Del Boccio[7,11], Dmitri V. Krysko[2,3,†], Luciana Dini[1], Stefano Tacconi[1]

Keywords:
Glioblastoma, extracellular vesicles, temozolomide, tumour microenvironment

Citation: Vardanyan D, Karimova M, Efimova I, Fratini F, Dinarelli S, Cufaro MC, Chieppa M, Zuccotti M, Alfieri A, Del Boccio P, Krysko DV, Dini L, Tacconi S. Temozolomide reshapes concentration, morphology, proteome, and biological activity of glioblastoma-derived extracellular vesicles. *Extracell Vesicles Circ Nucleic Acids.* 2026;7:1751-74. https://dx.doi.org/10.20517/evcna.2026.91

Received: 12 May 2026 **First Decision:** 22 Jul 2026 **Revised:** 2 Sep 2026 **Accepted:** 16 Sep 2026 **Published:** 16 Oct 2026

Academic Editors: Yoke Peng Loh, Shenglin Huang **Copy Editor:** Ting-Ting Hu **Production Editor:** Ting-Ting Hu



Abstract

Aim: Glioblastoma (GBM) is an aggressive brain tumour with poor prognosis and limited sensitivity to temozolomide (TMZ). GBM cells release extracellular vesicles (EVs) that shape the tumour microenvironment and can influence how the tumour responds to therapy. Here we examined how TMZ affects EV output from GBM cells and how these EVs act biologically on recipient GBM and immune cells.

Methods: EVs were isolated from four human GBM cell lines (U87MG, U251MG, U373MG, and T98G) cultured under control conditions or treated with TMZ. EVs were characterized for their morphology, size, and cargo composition. Functional assays evaluated EV uptake and their effects on cell death- and stress-associated markers in recipient GBM cells. The impact of EVs on dendritic and BV-2 microglial cells was also assessed. Proteomics data are available via ProteomeXchange (PXD070357).

Results: TMZ induced heterogeneous responses among GBM cell lines, confirming GBM

[1]Department of Biology and Biotechnologies "Charles Darwin", Sapienza University of Rome, Rome 00185, Italy.
[2]Cell Death Investigation and Therapy (CDIT) Laboratory, Anatomy and Embryology Unit, Department of Human Structure and Repair, Ghent University, Ghent 9000, Belgium.
[3]Cancer Research Institute Ghent, Ghent 9000, Belgium.
[4]Department of Neuroscience, Istituto Superiore di Sanità (ISS), Rome 00185, Italy.
[5]Institute for the Structure of Matter (ISM), National Research Council (CNR), Rome 00133, Italy.
[6]Department of Innovative Technologies in Medicine and Dentistry, G. d'Annunzio University of Chieti-Pescara, Chieti 66100, Italy.
[7]Center for Advanced Studies and Technology (CAST), Proteomics and Metabolomics Core Facility, G. d'Annunzio University of Chieti-

Pescara, Chieti 66100, Italy.
[8]Department of Environmental and Biological Science and Technology, University of Salento, Lecce 73100, Italy.
[9]Department of Biology and Biotechnology "Lazzaro Spallanzani", University of Pavia, Pavia 27100, Italy.
[10]Centro Grandi Strumenti, University of Pavia, Pavia 27100, Italy.
[11]Department of Science, G. d'Annunzio University of Chieti-Pescara, Chieti 66100, Italy.
[#]These authors contributed equally to this work.
[†]In memoriam.

Correspondence to: Prof. Luciana Dini, Dr. Stefano Tacconi, Department of Biology and Biotechnologies "Charles Darwin", Sapienza University of Rome, Rome 00185, Italy. E-mail: luciana.dini@uniroma1.it; stefano.tacconi@uniroma1.it

variability. TMZ differentially altered EV production, morphology, size, and protein cargo composition, particularly proteins associated with migration, invasiveness, immune regulation, and cell death. GBM cells efficiently internalized EVs, and EV treatment modulated cell death- and stress-associated markers regardless of TMZ exposure. Moreover, GBM-derived EVs promoted maturation of dendritic cells and activation of BV-2 microglial cells in cell type-dependent manner.

Conclusion: GBM-derived EVs act as regulators of tumour-microenvironment crosstalk and shape how cells respond to TMZ. These findings provide new insights into the complexity of EV-mediated signalling in GBM and improve our understanding of the mechanisms underlying tumour progression and treatment response.

INTRODUCTION

Glioblastoma (GBM) remains the most aggressive and treatment-refractory primary tumour of the central nervous system (CNS), with a median survival of approximately 15 months despite multimodal therapy[1]. Its dismal prognosis is largely attributable to its highly infiltrative growth pattern, which limits the possibility of complete surgical resection and reduces the effectiveness of conventional therapeutic strategies[2]. Clinical management is further complicated by the urgent need for intervention and by the limited number of agents capable of penetrating the blood-brain barrier (BBB) and reaching the tumour at therapeutically effective concentrations[3]. Although the current standard of care, consisting of maximal safe resection followed by radiotherapy and adjuvant temozolomide (TMZ), has improved patient outcomes, durable disease control remains uncommon[4]. Despite tremendous progress in basic research and clinical practice, a cure remains elusive due to the cellular and molecular heterogeneity of GBM, including the presence of cancer stem cells and different genetic alterations in known molecular pathways, such as receptor tyrosine kinase (RTK) signalling, p53 signalling, and Retinoblastoma protein (Rb)-mediated G1 checkpoint machinery[5], while mutations in isocitrate dehydrogenase (IDH) represent a unique signature in a distinct subset of gliomas[6,7].

GBM's highly heterogeneous tumour microenvironment (TME) adds to this complexity[8]. Beyond malignant cells, the GBM microenvironment comprises resident neural and immune populations, as well as infiltrating cells derived from the periphery that can cross the BBB, including bone marrow-derived immune cells[9]. The TME therefore represents a highly dynamic and plastic ecosystem, shaped by continuous changes in cellular composition, intercellular crosstalk, metabolic activity, and physicochemical conditions such as oxygen availability and pH[10]. Growing evidence indicates that this microenvironment is not merely a passive scaffold but an active determinant of glioblastoma behavior and treatment response[11].

Communication between GBM cells and the surrounding microenvironment occurs through both direct cell-cell contact and indirect signalling mediated by soluble factors and extracellular vesicles (EVs)[12]. EVs are membrane-enclosed particles released by virtually all cell types and detectable in a wide range of biological fluids. By transferring proteins, lipids, nucleic acids, and other bioactive molecules, they mediate both local and systemic signalling and contribute to communication between cells and with the extracellular

matrix[13]. Their molecular cargo is highly dependent on the physiological and pathological state of the donor cell and may be modulated by diverse chemical and physical stimuli[14,15]. Following their release, EVs interact with recipient cells through multiple classes of surface molecules, including tetraspanins, integrins, lectins, lipids, and extracellular matrix components, before being internalised and functionally reprogramming target cells[16,17]. In GBM, EVs have been shown to transport selective sets of microRNAs (miRNAs) and proteins, supporting their putative role as vectors of tumour cell survival, phenotypic plasticity, and microenvironmental remodelling[18].

EVs are commonly classified according to their biogenesis, size, and biological context. These categories include exosomes, generated as intraluminal vesicles (ILVs) within multivesicular bodies (MVBs) during endosomal maturation, and ectosomes, which arise through outward budding of the plasma membrane; additional subtypes include small and large EVs, migrasomes, oncosomes, and apoptotic bodies[19,20]. Another emerging and functionally relevant feature of EVs is the biomolecular corona, a dynamic layer of proteins, nucleic acids, and other biomolecules acquired in physiological and protein-rich environments. This corona can significantly influence EV biological activity, including processes related to regeneration, angiogenesis, and immune regulation[21-23].

Among the therapeutic challenges in GBM, resistance to TMZ remains particularly relevant[24]. Because of its lipophilic properties, TMZ efficiently crosses the BBB and therefore represents the backbone of chemotherapeutic treatment for this tumour. As research into the TME in gliomas has increased, so too has interest in EVs as a means of understanding their contribution to promoting or hindering tumour progression. Based on these considerations and additional evidence from other cancer types[25,26], TMZ treatment may interfere with EV production by GBM cells within the TME, thereby affecting the GBM's response to the drug. Considering the extreme heterogeneity of GBM tumours, this study aims to determine whether EVs are affected in terms of morphology, concentration, cargo composition, and biological effects by TMZ treatment of donor cells and, in turn, influence TMZ-induced cell death and migratory activity of recipient cells. To this end, four human IDH-wildtype GBM cell lines (U87MG, U251MG, U373MG, and T98G), which differ in their molecular profiles and sensitivity to TMZ, were selected[27-29].

METHODS

Cell culture

Human U87MG, U251MG, U373MG, and T98G GBM cell lines, and murine microglial BV-2 cells were cultured in Dulbecco's Modified Eagle Medium (DMEM) 4.5 g/L glucose (Sigma Aldrich, St. Louis, MO) supplemented with 10% heat-inactivated fetal bovine serum (FBS; Sigma Aldrich, St. Louis, MO), 1% L-glutamine (Corning, Manassas, VA), 1% penicillin and streptomycin solution (Corning, Manassas, VA), and 1% amphotericin B (Sigma Aldrich, St. Louis, MO). Cells were cultured in a 5% CO_2 humidified atmosphere at 37 °C. Cells were maintained in T75 flasks (75 cm^2) at a seeding density of 2 × 10^6 cells per flask and subcultured three times per week upon reaching approximately 80% confluence. U87MG ATCC [Research Resource Identifier (RRID): CVCL_0022], U251MG (RRID: CVCL_0021), U373MG Uppsala (RRID: CVCL_2818), T98G (RRID: CVCL_0556), and BV-2 (RRID: CVCL_0182) cell lines were obtained from the Cell Bank, IRCCS AOU San Martino-IST (Genova, Italy). All cell lines were tested for mycoplasma contamination by polymerase chain reaction (PCR) every 3 weeks and were confirmed to be mycoplasma-free throughout the study. All cell lines were used between passages 1 and 5, except T98G, which has a stable profile and was used between passages 1 and 25.

Isolation and differentiation of bone marrow-derived dendritic cells (BMDCs)

Bone marrow from 6-8 week-old female C57BL/6J mice was isolated from femurs and tibias as reported in[30] and cultured in Roswell Park Memorial Institute medium (RPMI) medium (ThermoFisher Scientific, Waltham, MA) supplemented with 5% heat-inactivated fetal calf serum, 20 ng/mL murine

colony-stimulating factor (CSF) (UGent-IRC-VIB Protein Core Facility, Ghent, Belgium), 1% L-glutamine, and 50 μM 2-mercaptoethanol (ThermoFisher Scientific, Waltham, MA). In total, three animals (n = 3) were used as three independent biological replicates. The bone marrow was flushed with a 25 G needle (0.5 mm × 25 mm), resuspended, and coarse debris filtered through a CellStrainer 70 μm (ThermoFisher Scientific, Waltham, MA) and cleared from red blood cells using red blood cell (RBC) Lysis buffer 1X (ThermoFisher Scientific, Waltham, MA). Cells were cultured for up to 10 days. The culture medium was replaced with fresh medium on days 3, 6, and 9. All animal experiments were approved by the Animal Ethical Committee of the Faculty of Medicine and Health Sciences of Ghent University (approval/accreditation number: LA1400080; project reference: ECD 20/06aanp).

MTT assay and TMZ treatments

Cell viability was evaluated with the 3-(4,5-dimethylthiazol-2-yl)-2,5-diphenyltetrazolium bromide (MTT) assay following the modified protocol of Sladowski *et al.*[31]. U87MG, U251MG, U373MG, and T98G cells (1 × 10^4 cells/100 μL/well) were seeded into 96-well plates and exposed to TMZ (100, 200, 400, and 800 μM) (ThermoFisher Scientific, Waltham, MA) for 24, 48, and 72 h. Cells were then incubated with 1 mg/mL of MTT (PanReac AppliChem, Darmstadt, Germany) in DMEM for 3 h at 37 °C and 5% CO_2, washed three times with phosphate-buffered saline (PBS; Aurogene, Rome, Italy) and lysed with dimethyl sulfoxide (DMSO; ThermoFisher Scientific, Waltham, MA) to dissolve the formazan crystals. Absorbance was read at 570 nm on a Multiskan™ FC Microplate Photometer (ThermoFisher Scientific, Waltham, MA).

Crystal violet cell viability assay

U87MG and U251MG cells (1 × 10^4 cells/100 μL/well) were seeded into 96-well plates and exposed to TMZ (100, 200, 400, and 800 μM) for 48 h. Cells were then fixed with 4% paraformaldehyde (PFA; Sigma-Aldrich, St. Louis, MO) in PBS (30 min, RT), stained with 0.1% crystal violet (Sigma-Aldrich, St. Louis, MO) [1 h, room temperature (RT)], rinsed with water, and air-dried. Bound dye was solubilized in glacial acetic acid (Sigma-Aldrich, St. Louis, MO), and absorbance was measured at 550 nm with a Multiskan™ FC Microplate Photometer.

EV isolation by ultrafiltration combined with size exclusion chromatography (UF/SEC)

EVs were isolated from conditioned media of cells treated with 200 μM TMZ for 48 h in EV-depleted 10% FBS-supplemented DMEM. After sequential centrifugation to remove cells and debris, the medium was concentrated using 10 kDa molecular weight cut-off (MWCO) Amicon Ultra-15 filters at 4,000 × g (Merck Millipore, Burlington, MA), and EVs were purified by SEC using a 10 mL Sepharose CL-2B column (Cytiva, Uppsala, Sweden), as reported in[32]. EV-rich, protein-poor fractions (from 8 to 10) were collected in PBS and further concentrated to 100 μL with Amicon Ultra-4 filters (10 kDa MWCO; Merck Millipore, Burlington, MA) at 4,000 × g for 20 min.

Nanoparticle tracking analysis (NTA)

EV size and concentration were assessed by NTA using a NanoSight® NS300 (Malvern Panalytical Ltd., Malvern, UK), equipped with a 488 nm blue laser and a high-sensitivity sCMOS camera. Recordings were analysed with NTA 3.4 Build 3.4.4 software (Malvern Panalytical Ltd., Malvern, UK). Samples were diluted 1:50 in freshly filtered PBS, vortexed for 1 min, and injected using a syringe pump at 30 arbitrary units (AU). For each of the three independent biological replicates, five 1-min videos were recorded and analysed to determine particle concentration (particles/mL), size distribution, mean, mode, standard deviation, diameter distributions (D10, D50, D90), and valid tracks.

Transmission electron microscopy (TEM) analysis

For TEM analysis, untreated and TMZ-treated GBM cells were fixed for 1 h with 2.5% glutaraldehyde (Electron Microscopy Sciences, Hatfield, PA) in 0.1 M cacodylate buffer pH 7.4 (Sigma-Aldrich, St. Louis, MO) and post-fixed for 2 h with 1% osmium tetroxide (OsO_4; Electron Microscopy Sciences, Hatfield, PA) in

the same buffer, dehydrated in ethanol, embedded in Spurr's resin (Electron Microscopy Sciences, Hatfield, PA), sectioned into 60 nm slices (ultramicrotome RMC Boeckeler, Tucson, AZ), and placed on 200-mesh copper grids (Ted Pella, Inc., Redding, CA). For isolated EVs, samples were fixed with 0.1% PFA in PBS for 30 min at RT, loaded onto 200-mesh Formvar/carbon-coated grids (Ted Pella, Inc., Redding, CA), stained with 2% uranyl acetate (Electron Microscopy Sciences, Hatfield, PA, USA), and all samples were examined using a Zeiss Auriga Scanning Electron Microscope (Carl Zeiss Microscopy GmbH, Jena, Germany) equipped with the STEM module, operating at 20 keV.

Cryo-electron microscopy (cryo-EM) analysis

Cryo-EM samples of EVs were prepared as described in[33]. Briefly, a 4 μL aliquot of each EV sample was applied to glow-discharged grids, followed by blotting and plunge-freezing in liquid ethane. Glacios cryo-transmission electron microscope (ThermoFisher Scientific, Waltham, MA) was used to collect micrographs.

Immunogold labelling for CD63

Fixed EV samples were loaded on 200-mesh Formvar/carbon-coated grids by inversion and then floated sequentially on droplets of PBS (three times for 3 min), 0.5% bovine serum albumin (BSA; Sigma-Aldrich, St. Louis, MO) in PBS (10 min), primary antibody anti-CD63 (60 min; 1:500 in PBS with 5% BSA, #sc-365604; Santa Cruz Biotechnology, Dallas, TX), 1% BSA (six times for 3 min), 20 nm protein A-gold conjugate (40 min; Abcam, Cambridge, UK; ab270601), 1% BSA (three times for 3 min) and, finally, washed in PBS (three times for 3 min). Then, grids were contrasted in 2% uranyl acetate (7 min, RT) and observed under a Zeiss Auriga Scanning Electron Microscope (Carl Zeiss Microscopy GmbH, Jena, Germany) equipped with the STEM module, operating at 20 keV.

Atomic force microscopy (AFM)

AFM analysis of GBM cells and isolated EVs was performed as previously described by our group[34], with minor adaptations. Briefly, GBM cells (5×10^4 cells/well) were seeded on glass coverslips in 6-well plates, treated as required, and fixed on ice for 30 min with 1% glutaraldehyde in 0.1 M cacodylate buffer (pH 7.4), then air-dried at RT for 1 h. Isolated EVs were fixed with 0.1% PFA in PBS (30 min, RT) and diluted in Milli-Q water. Images were acquired in contact mode on a Multimode AFM (Bruker, Santa Barbara, CA) using DNP-model cantilever tips (Bruker; nominal spring constant 0.06 N/m, tip radius 10 nm), keeping the tip-sample force below 1 nN. Cells were scanned at 60 μm with 20 μm zoom-ins on areas of interest, while EVs were imaged at 20 μm and, more extensively, at 10 μm until enough vesicles were captured (scan speed 1-4 s/line, ≥ 512 points/line). Images were processed in Gwyddion (mean-plane subtraction, tilt correction, line-levelling), and vesicles were segmented and counted using the "Mark Grains by Segmentation" tool. Surface roughness (Rq) was calculated in ImageJ v1.8.0[35] on five randomly selected 6 μm^2 × 6 μm^2 regions per sample.

Western blot analysis

Cells were lysed in radioimmunoprecipitation assay (RIPA) buffer (NaCl 150 mM, Tris-HCl 50 mM pH 8, $MgCl_2$ 2 mM, sodium dodecyl sulfate (SDS) 0.1%, deoxycholic acid 0.5%, NP-40 1%; Sigma-Aldrich, St. Louis, MO) containing phenylmethylsulfonyl fluoride (PMSF) and protease inhibitor cocktail (ThermoFisher Scientific, Waltham, MA). After sonication (5 min), insoluble material was pelleted by centrifugation for 30 min at 13,000 × *g* at 4 °C. Supernatants were transferred to a new tube, and the protein concentration was measured by Bradford assay using Bradford reagent (Bio-Rad Laboratories, Hercules, CA). 15-30 μg of protein was separated by SDS-polyacrylamide gel electrophoresis (10%-12% polyacrylamide; SureCastTM Acrylamide Solution; ThermoFisher Scientific, Waltham, MA) and transferred to nitrocellulose membranes (Bio-Rad Laboratories, Hercules, CA). For Western blot analysis of EVs, 10 μg of proteins from the EV-enriched fractions were used. The membranes were blocked with 5% non-fat dry milk (PanReac

AppliChem, Darmstadt, Germany) and/or 3% BSA (blocking buffer) in Tris-buffered saline containing 0.1% Tween 20 (TBST; Sigma-Aldrich, St. Louis, MO) for 1 h at RT. Then, the membranes were incubated overnight at 4 °C with the following primary antibodies: tumor susceptibility gene 101 (TSG101) (1:1,000 dilution, #sc-7964; Santa Cruz Biotechnology, Dallas, TX), CD63 (1:1,000 dilution, #sc-365604; Santa Cruz Biotechnology, Dallas, TX), and ALG-2-interacting protein X (ALIX) (1:1,000 dilution, #sc-53540; Santa Cruz Biotechnology, Dallas, TX) diluted in blocking buffer. After washing with TBST, the membranes were incubated for 1 h at RT with a goat anti-mouse IgG Heavy and Light Chain secondary antibody (1:5,000, #A90-116P; Bethyl Laboratories, Montgomery, AL) diluted in blocking buffer. The immunoreactive bands were detected with a ChemiDoc imaging system (Bio-Rad Laboratories, Hercules, CA) using commercial enhanced chemiluminescence (ECL) reagent (WesternBrightTM Quantum, Advansta Inc., San Jose, CA). To check cell death, the membranes were incubated overnight at 4 °C with the following primary antibodies: caspase-3 (1:1,000 dilution, A19654, ABclonal, Wuhan, China), caspase-8 (1:1,000 dilution, A19549, ABclonal, Wuhan, China), caspase-9 (1:1,000 dilution, A18676, ABclonal, Wuhan, China), LC3B (1:1,000 dilution, A19665, ABclonal, Wuhan, China), glutathione peroxidase 4 (GPX4) (1:1,000 dilution, A11243, ABclonal, Wuhan, China), and β-actin (1:1,000 dilution, #bs-0061R, Bioss, Beijing, China) diluted in blocking buffer. To check BV-2 activation, the membranes were incubated with the following primary antibodies: CD80 (1:1,000 dilution, A16039, ABclonal, Wuhan, China) and CD206 (1:1,000 dilution, A11192, ABclonal, Wuhan, China). After washing with TBST, the membranes were incubated for 1 h at RT with a Goat anti-Rabbit IgG Heavy and Light Chain secondary antibody (1:5,000 dilution, #A120-101P, Bethyl Laboratories, Montgomery, AL) diluted in blocking buffer.

Label-free proteomics and bioinformatics analysis

To profile the EV protein cargo, SEC-purified EVs from three independent biological replicates of T98G, U87MG, U251MG and U373MG cells were pooled, sonicated on ice (Sonicator U200S, 70% amplitude; IKA Labortechnik, Staufen, Germany) and processed by Filter-Aided Sample Preparation (FASP). Tryptic digests (15 µg protein/sample, Bradford-verified) were analysed in triplicate on a ultimate™ 3000 ultra-high performance liquid chromatography (UHPLC) coupled to an Orbitrap Fusion™ Tribrid™ mass spectrometer (both ThermoFisher Scientific, Waltham, MA), following the chromatographic set-up previously described[36], peptides loaded on a Trap Cartridge C18 (0.3 mm ID, 5 mm L, 5 µm PS) and resolved on an EASY-spray Acclaim™ PepMap™ C18 column (75 µm ID, 15 cm L, 2 µm PS; both ThermoFisher Scientific) at 300 nL/min over a 65-min run. Raw data were processed in MaxQuant 1.6.6.0 and Perseus 1.6.10.50 (Max Planck Institute for Biochemistry, Martinsried, Germany) against the UniProt Homo sapiens database (release 2020_06, 20,588 entries), as reported previously[37]: cysteine carbamidomethylation was fixed, methionine oxidation and asparagine/glutamine deamidation were variable, and false discovery rate (FDR) was capped at 1% at both protein and peptide level. Protein abundance was estimated via intensity-based absolute quantification (iBAQ) values, requiring ≥ 2 valid values in at least one treatment group per comparison. Differential protein ratios (TMZ-treated *vs.* untreated) were analysed for gene ontology (GO) and functional enrichment using Ingenuity Pathway Analysis (IPA, Qiagen, Hilden, Germany; accessed February 2025), which predicts activation ($z \geq 2.0$) or inhibition ($z \leq -2.0$) of transcriptional regulators based on curated literature evidence[38]. Proteomics data were deposited in the ProteomeXchange Consortium via PRoteomics IDEntifications database (PRIDE) (dataset PXD070357)[39].

PKH26 labelling and EV uptake experiments

EVs were labelled with PKH26 Red Fluorescent Cell Linker Kits for General Cell Membrane Labeling (Sigma-Aldrich, St. Louis, MO) according to the manufacturer's instructions. 1 mL EV sample (volume adjusted with diluent C) and 6 µL of PKH26 dye were mixed, gently pipetted for 30 s, and then left at RT for 5 min. The excess dye was removed by a second SEC purification. PKH26-only controls were processed, with

PBS substituting the EV sample. 5 × 10^5 of GBM cells, BMDCs, or BV-2 cells were then exposed to PKH26-labelled EVs (4 μg/mL), fixed at different time points (30 min, 1, 3, and 24 h) with 4% PFA, washed twice with PBS and blocked with 5% BSA in PBS, and then samples were stained for β-actin (1:200; AC004, ABclonal, Wuhan, China), washed twice with PBS and incubated with secondary Goat Anti-Mouse IgG H&L fluorescein isothiocyanate (FITC)-conjugated antibody (1:400; ab6785, Abcam, Cambridge, UK). Finally, nuclei were stained with 4',6-diamidino-2-phenylindole (DAPI) Fluoromount-G (SouthernBiotech, Birmingham, AL). EV uptake was examined by confocal laser scanning microscopy (Leica Geosystems, Wetzlar, Germany) or Axio Imager M2 equipped with Apotome 2 (Zeiss GmbH, Jena, Germany). Z-stack imaging was used to distinguish internalized EVs from surface-bound EVs. Images were analysed using ImageJ Software version 1.54p[34].

Incubation of GBM cells, BMDCs, and BV-2 cells with EVs

A total of 5 × 10^5 cells per well of U87MG, U251MG cells, BMDCs, or BV-2 cells were seeded in 6-well plates and treated with 4 μg/mL of EVs in EV-depleted medium for 24 h. After the treatments, cells were processed for all subsequent functional analyses.

Wound healing assay

T98G, U87MG, U251MG, and U373MG cells were seeded at a density of 5 × 10^5 cells/well into 6-well plates, and a scratch after 24 h was made in the centre of each well using a 200 μL pipette tip to assess migration. After washing out debris, cells were treated with 200 μM TMZ in 1% FBS-supplemented medium or with EVs from U87MG and U251MG cells in EV-depleted 1% FBS-supplemented medium. Wound closure was monitored over time (0, 1, 3, 6, 12, and 24 h, and additionally at 48 and 72 h for U251MG) by bright-field microscopy (Zeiss GmbH, Jena, Germany). Cell migration was quantified as gap area in at least three random fields using the MRI Wound Healing Tool plugin in ImageJ 1.53 software[34].

Flow cytometry

To examine the effect of EVs derived from GBM cells on BMDC maturation, isolated EVs from both TMZ-treated and untreated U87MG and U251MG cells were added to the dendritic cells (DCs) starting from day 7 of culture for 24 h. Lipopolysaccharide (LPS; 1 μg/mL, *Escherichia coli* O111:B4; Sigma-Aldrich, St. Louis, MO) was added for an additional 24 h. LPS without EVs was used as a positive control, while untreated cells were used as a negative control. Both adherent and suspended cells cultured by the above methods were harvested from 6-well plates and centrifuged at 500 × *g* for 5 min at 4 °C. After centrifugation, the cells were washed and resuspended in fluorescence-activated cell sorting (FACS) buffer. Next, DCs were incubated for 20-30 min with the following antibodies: eFluor 450-conjugated anti-CD86 (clone GL1; eBioscience, San Diego, CA), Alexa Fluor 488-conjugated anti-major histocompatibility complex-II molecule (MHCII/IA-IE clone M5/114.15.2; BD Biosciences, San Jose, CA), eFluor 450-conjugated anti-CD80 (clone 16-10A1; eBioscience, San Diego, CA), allophycocyanin (APC)-conjugated anti-CD11c (clone N418, eBioscience, San Diego, CA), and mouse Fc-blocker (clone 93, eBioscience, San Diego, CA). After incubation, cells were washed with PBS by centrifugation at 300 × *g* for 5 min at 4 °C. The supernatant was removed, and the cells were resuspended in 200 μL of PBS. Flow cytometric analyses were performed with a BD LSR II flow cytometer (BD Biosciences, San Jose, CA) at the UGent Core Flow Cytometry facility of Ghent University. At least 10,000 events were recorded for each sample. In all the analyses, debris and clumps were gated out. The data were analysed with FlowJo Flow Cytometry Analysis Software (TreeStar Inc., Ashland, OR).

Quantitative reverse transcription PCR (RT-qPCR)

Total RNA was extracted by TRI-TIZ G (PanReac AppliChem, Darmstadt, Germany), and 1 μg RNA was used to generate complementary DNA using the SensiFAST complementary DNA (cDNA) synthesis kit (Meridian Bioscience, London, UK) according to the manufacturers' protocols. The resulting cDNA was

used for qPCR with SensiFAST Probe Lo-ROX kit (Meridian Bioscience, London, UK) with the following primer pairs: Tbp (Forward primer TGGAATTGTACCGCAGCTTCAAAAT; Reverse primer GCAGTTGTCCGTGGCTCTCT), IL-1β (Forward primer TGCCACCTTTTGACAGTGATGA; Reverse primer TGCCTGCCTGAAGCTCTTGT), IL-10 (Forward primer TAGAAGTGATGCCCCAGGCAG; Reverse primer ACACCTTGGTCTTGGAGCTTATT), and analysed with QuantStudio™ 3 Real-Time PCR System (Applied Biosystems, ThermoFisher Scientific, Waltham, MA). Relative gene expression levels were calculated with the ΔΔCT method.

Statistical analysis

All data are expressed as mean ± standard deviation (SD) of at least three indipendent biological replicates. Multiple comparisons were performed using either one-way analysis of variance (ANOVA) followed by Tukey's post hoc test or by two-way ANOVA. Comparisons between two groups were performed using Student's *t*-test. Statistical analyses were performed using GraphPad Prism 7 (GraphPad Software, San Diego, CA), and $P < 0.05$ was considered statistically significant.

RESULTS

Heterogeneous populations of EVs in terms of size and concentration are released by the different GBM cell lines

Firstly, TEM analysis was used to identify MVBs and budding EVs in all four human GBM cell lines. MVBs with ILVs and plasma membrane budding were observed in all GBM cell types, with no significant differences in the size or number of MVBs [Figure 1A]. Next, EV-enriched fractions from the four GBM cell lines were isolated using UF/SEC. EV morphology was assessed using TEM, cryo-EM, and AFM [Figure 1B-D]. TEM micrographs revealed EVs with a characteristic round, cup-shaped morphology, with sizes ranging from 20 to 160 nm for T98G, U87MG, and U373MG-derived EVs, and from 10 to 180 nm for U251MG-derived EVs [Figure 1B and Supplementary Figure 1A]. Cryo-EM analysis revealed EVs in a near-native morphological state, predominantly round and enclosed by clearly visible lipid bilayers [Figure 1C]. Importantly, no round, moderately electron-dense lipoproteins lacking a lipid bilayer were detected. This confirms the success of the isolation protocol[33]. In addition, a well-established AFM protocol from our group was used[35], which corroborated these morphological features [Figure 1D] and provided more statistically reliable information. Specifically, AFM-based analysis confirmed the size range previously observed by TEM: EVs isolated from T98G, U87MG, and U373MG cells ranged from 50 to 200 nm, while EVs derived from U251MG cells exhibited a broader size distribution, extending up to 350 nm. The concentration and size distribution of EVs derived from GBM cell lines were also analysed by NTA [Figure 1E and Supplementary Figure 1B]. All EVs ranged from 40 to 300 nm, with T98G-, U87MG-, and U251MG-derived EVs showing a larger modal diameter of approximately 120 nm, while U373MG-derived EVs had a smaller modal diameter of 90 nm [Figure 1E]. In addition, particle concentration varied among EVs from the different GBM cell lines, with the highest concentration measured for T98G [Supplementary Figure 1B]. Finally, the presence of the main EV markers, such as CD63, TSG101, and ALIX, was assessed using Western blot analysis [Figure 1F]. All EV preparations expressed the analysed markers. CD63 was also detected at the ultrastructural level using immunogold labelling, as illustrated in Figure 1G.

TMZ affects the morphology, concentration, and protein cargo composition of GBM-derived EVs

To evaluate TMZ effects on EV release from GBM cells, we first determined the minimum TMZ concentration required to induce cellular stress while maintaining EV production. In line with the Minimal Information for Studies of Extracellular Vesicles (MISEV) guidelines[19], it is crucial to prevent the contamination of EV samples with apoptotic bodies. Therefore, the sensitivity of various GBM cell lines (T98G, U87MG, U251MG, and U373MG) to TMZ was evaluated using time- and concentration-dependent analyses with the MTT assay. As shown in Figure 2A-D, cell viability was not affected after 24 h of treatment

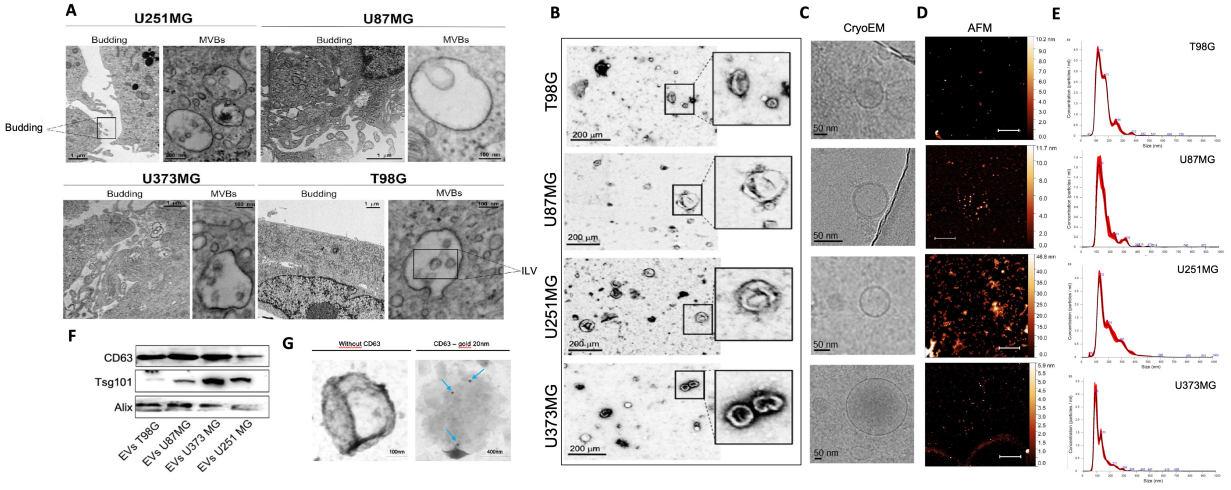


Figure 1. Ultrastructural characterization of GBM cells and GBM-derived EVs. (A) TEM micrographs showing budding vesicles and MVBs with ILVs in U251MG, U87MG, U373MG, and T98G cells; (B) TEM, (C) cryo-EM, and (D) AFM representative images of isolated EVs from T98G, U87MG, U251MG, and U373MG cells. AFM images scale bar: 20 µm; (E) Size distribution of EVs isolated from T98G, U87MG, U251MG, and U373MG cells measured by NTA; (F) Representative Western blot of CD63, TSG101, and ALIX in EV-enriched fractions isolated from T98G, U87MG, U251MG, and U373MG cells; (G) Representative TEM images of isolated EVs with immunogold enhancement with anti-CD63; blue arrows indicate Protein A-gold particles bound to the anti-CD63 antibody, labeling CD63-positive EVs. AFM: Atomic force microscopy; ALIX: ALG-2-interacting protein X; CD63: cluster of differentiation 63; cryo-EM: cryo-electron microscopy; EVs: extracellular vesicles; GBM: glioblastoma; ILVs: intraluminal vesicles; MVBs: multivesicular bodies; NTA: nanoparticle tracking analysis; TEM: transmission electron microscopy; TSG101: tumor susceptibility gene 101.

in all four GBM cell lines, whereas a similar decrease in cell viability was observed after 48 and 72 h. Based on these results, treatment with 200 µM TMZ for 48 h was selected for all four GBM cell lines for further investigation of the effects of TMZ on GBM cells and GBM-derived EVs, as this condition did not promote overt cell death. The results obtained using the MTT assay were further validated by a crystal violet cell viability assay, as reported in Supplementary Figure 2. The impact of TMZ on zonal budding distribution on the cell surface was evaluated using a well-established AFM-based approach from our group[35]. As shown in Figure 2E-I and Supplementary Figure 1C, TMZ treatment resulted in increased Rq, which correlates with budding abundance[35], at the perinuclear/cellular edge (PNu/CE) area in U251MG and U373MG cells. By contrast, U87MG cells exhibited reduced budding within the nuclear (Nu) region [Figure 2G], whereas T98G cells displayed decreased budding in the Nu region and increased budding at the PNu/CE [Figure 2F]. The effects of TMZ treatment on the size, concentration, and morphology of isolated EVs from all GBM cell lines were analysed. AFM analysis revealed that TMZ treatment increased the mean size of EVs released by U251MG and U373MG cells [Figure 2J and K], while no variation was observed for U87MG cells. Conversely, TMZ treatment reduced the mean diameter of T98G-derived EVs [Figure 2J and K]. Furthermore, NTA analysis revealed a decrease in particle concentration in both T98G- and U251MG-derived EVs under TMZ treatment, with the opposite trend observed for U87MG- and U373MG-derived EVs [Figure 2L and Supplementary Figure 1D]. Morphologically, cryo-EM imaging [Figures 1C and 2M] showed that EVs from both TMZ-treated and untreated cells contained multilayered vesicles, though the relative percentage increased in EVs from treated cells (about 3% CTRL *vs.* 8% TMZ-treated cells).

Having determined the distinct morpho-dimensional changes induced by TMZ treatment, the effects of the chemotherapeutic agent on the protein cargo of GBM-derived EVs were analysed using label-free quantitative proteomics [Figure 3A-C]. Proteins from EV-SEC fractions of cell-free, depleted culture medium were used as negative controls (see Supplementary Table 1 "CTRL medium" column). As shown in the Venn diagrams of Figure 3A, a total of 84 and 86 proteins were robustly quantified for T98G-derived EVs from TMZ-treated and untreated cells, respectively. For U251MG-derived EVs, 56 proteins were identified

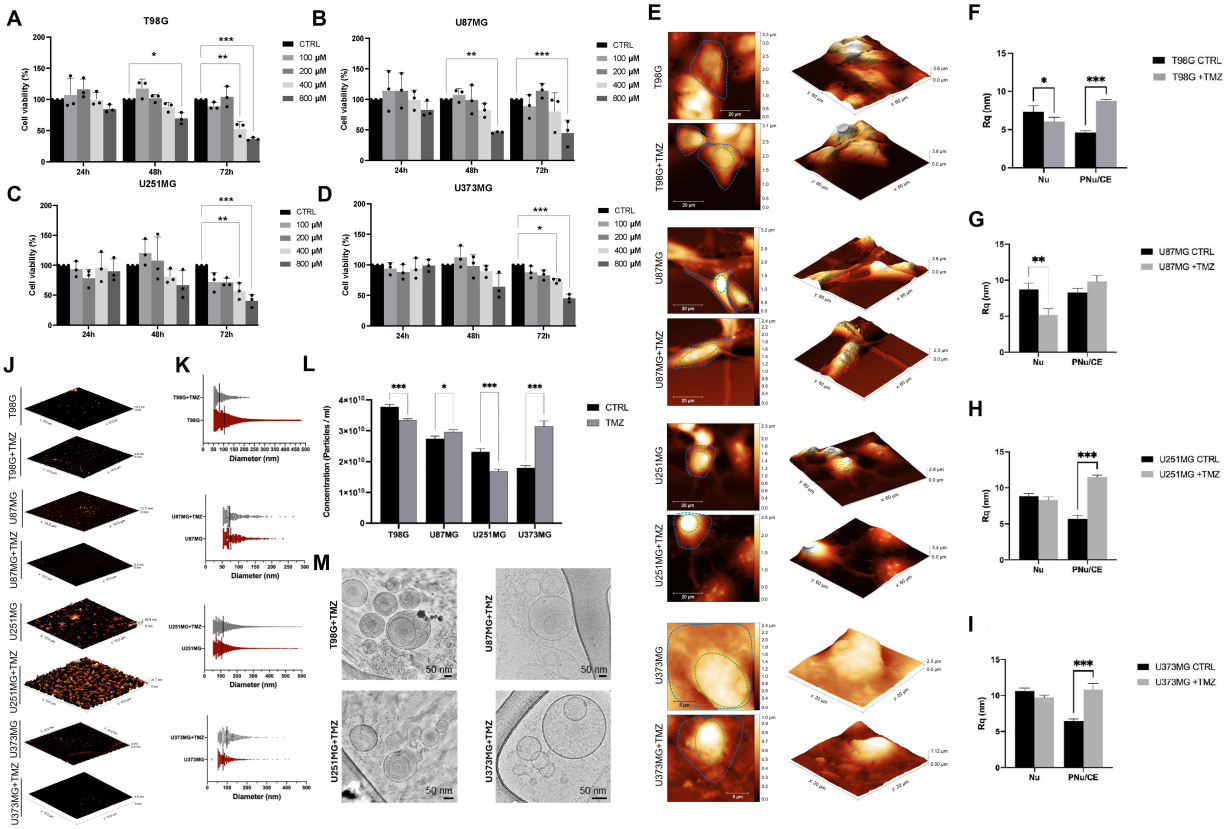


Figure 2. Effects of TMZ treatment on GBM cells and GBM-derived EVs. Cell viability was assessed by MTT assay in (A) T98G, (B) U87MG, (C) U251MG, and (D) U373MG cells treated with 100, 200, 400, or 800 µM TMZ for 24, 48, or 72 h. Data are reported as a percentage compared to the control (untreated cells; CTRL), presented as mean ± SD of three independent biological replicates ($n = 3$). $^{*}P < 0.05$, $^{**}P < 0.01$, $^{***}P < 0.001$ *vs.* control (Student's *t*-test); (E) Representative AFM images of CTRL (untreated) or TMZ-treated T98G, U87MG, U251MG, and U373MG cells. The Nu and PNu/CE areas are highlighted by green- and blue-dotted lines, respectively; Quantitative value of Rq measured in the Nu and PNu/CE area of CTRL or TMZ treated (F) T98G, (G) U87MG, (H) U251MG, and (I) U373MG cells; (J) Representative 3D reconstruction from AFM images of isolated EVs and (K) relative diameter measurements (mean diameter is shown as a black dotted line) of CTRL or TMZ-treated T98G, U87MG, U251MG, and U373MG; (L) Particle concentration measured by NTA. Data are presented as mean ± SD of three independent biological replicates ($n = 3$); $^{*}P < 0.05$, $^{***}P < 0.001$ *vs.* control (Student's *t*-test); (M) Cryo-EM images of EVs isolated from T98G, U87MG, U251MG, and U373MG cells treated with TMZ. AFM: Atomic force microscopy; cryo-EM: cryo-electron microscopy; CTRL: control; GBM: glioblastoma; MTT: 3-(4,5-dimethylthiazol-2-yl)-2,5-diphenyltetrazolium bromide; NTA: nanoparticle tracking analysis; Nu: nuclear region; PNu/CE: perinuclear/cellular edge; Rq: root mean square roughness; SD: standard deviation; TMZ: temozolomide.

in the TMZ-treated condition and 53 in the untreated condition. In U373MG-derived EVs, 162 proteins were quantified following TMZ treatment, compared with 42 proteins in the untreated condition. Lastly, 176 proteins were quantified in EVs released by TMZ-treated U87MG cells and 68 in the untreated condition. The details of the entire quantified protein dataset for each sample are reported in Supplementary Table 1, with protein abundances expressed as iBAQ values. Figures 3A and B demonstrate that TMZ treatment did not significantly impact the protein cargo of T98G-derived EVs, which shared 66.3% of proteins with EVs from untreated cells. These data were confirmed by univariate statistical analysis, as illustrated by the volcano plot [Figure 3B], which showed only minor changes in the EV protein cargo of T98G-derived EVs between the two conditions. In contrast, EVs isolated from TMZ-treated U87MG, U373MG, and U251MG cells exhibited marked alterations in their protein cargo. Specifically, U87MG- and U373MG-derived EVs contained substantially more quantified proteins than EVs from untreated cells, while volcano plot analysis revealed that the majority of differentially expressed proteins were significantly upregulated following TMZ treatment (red dots in Figure 3B). Similarly, U251MG-derived EVs were packaged with a specific set of proteins that were significantly upregulated after TMZ treatment. The complete list of differentially expressed proteins is reported in Supplementary Table 1.

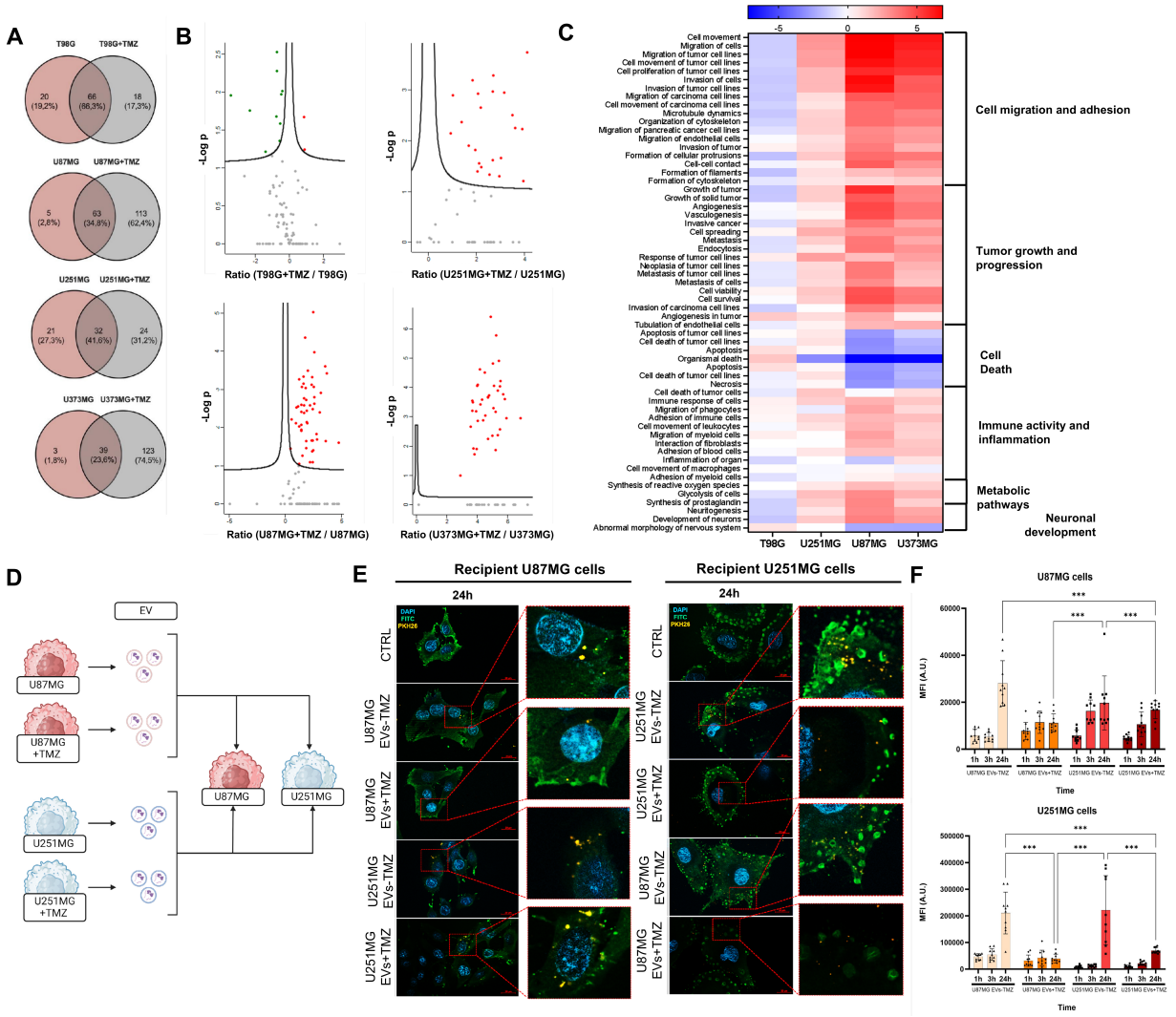


Figure 3. Effects of TMZ on the protein cargo of GBM-derived EVs and their internalisation in recipient GBM cells. (A) Venn diagrams show the quantified proteins in EVs derived from the four GBM cell lines, comparing TMZ-treated and untreated conditions (EVs +TMZ *vs.* EVs -TMZ); (B) Volcano plots showing DEPs identified in comparisons between TMZ-treated and untreated conditions (EVs +TMZ *vs.* EVs -TMZ). Data are graphed as ratios and -log(*P*-value): grey dots represent proteins not differentially expressed in the comparison; red dots represent significantly upregulated proteins, and green dots indicate proteins that were significantly downregulated in EVs isolated from TMZ-treated cells. Data are presented as mean ± SD of three independent biological replicates ($n = 3$). Statistical significance was determined using Student's *t*-test, with *P*-value < 0.05 considered statistically significant; (C) Heatmap of the main downstream effects predicted by the IPA tool in the performed comparisons. Data are graphed by z-score values, as shown in the legend above (red for activation and blue for inhibition). Biofunctions are grouped into larger biological categories; (D) Schematic representation of the treatments of recipient GBM cells with EVs from untreated or TMZ-treated U87MG and U251MG cells performed in this study; (E) Microscopy fluorescence images showing the uptake of PKH26-labelled EVs from untreated and TMZ-treated U87MG and U251MG cells in recipient GBM cells after 24 h of incubation (representative images at 1 and 3 h, together with PKH26-only controls are provided in Supplementary Figure 3); (F) Quantitative analysis of the MFI of internalised PKH26-labelled EVs in recipient U87MG and U251MG cells after 1, 3, and 24 h of incubation, measured using ImageJ Software version 1.54p[35]. Statistically significant differences between groups were determined using one-way ANOVA followed by Tukey's post hoc test ***$P < 0.001$. Data are presented as mean ± SD of three independent biological replicates ($n = 3$). ANOVA: Analysis of variance; DEPs: differentially expressed proteins; EVs: extracellular vesicles; GBM: glioblastoma; IPA: Ingenuity Pathway Analysis; MFI: mean fluorescence intensity; TMZ: temozolomide.

To further investigate the biological effects mediated by EV proteins derived from TMZ-treated GBM cells, the protein ratios (TMZ-treated/untreated) for each GBM cell line were analysed using the IPA tool (accessed in February 2025) to perform GO enrichment analysis, which highlights the significantly

modulated biological functions and molecular pathways in which proteins identified in GBM-derived EVs were involved. Figure 3C presents the main significant biological functions and processes as a heatmap, with z-score values shown in red and blue to indicate significant activation and inhibition, respectively, for each comparison between EVs isolated from TMZ-treated and untreated cells. In this context, the functions related to cell migration, adhesion, invasiveness, proliferation, and immune modulation, all processes necessary for tumour progression, were significantly higher in EVs derived from TMZ-treated U87MG and U373MG cells (see the most intense red colouring, which is related to higher and more positive z-score values). In contrast, cell death was significantly reduced in the same comparisons (see the most intense blue colouring related to lower and more negative z-score values). In U251MG cells, the function related to cell migration was also significantly modulated, but to a lesser extent compared with U87MG and U373MG cells. No significant modulation of functions related to proliferation, invasiveness, or immune response was observed in EVs isolated from T98G and U251MG cells, as indicated by the lighter colours of the heatmap boxes. Supplementary Table 1, sheet "downstream", reports the complete list of downstream effects for each comparison performed with z-score values (TMZ-treated *vs.* untreated).

In line with the MTT assays and proteomics results, the U87MG cell line (which showed the greatest sensitivity to TMZ treatment) and the U251MG cell line (which showed the lowest sensitivity to TMZ treatment) were selected for all subsequent functional analyses. Furthermore, the proteins involved in cell death processes were downregulated by TMZ treatment in U251MG-derived EVs, whereas they remained almost identical to those in EVs derived from untreated U87MG cells. For this reason, all subsequent functional investigations, including migratory activity, cell death, and immune maturation/activation, were conducted using these two cell lines and EVs derived from them. To this end, EVs isolated from U87MG and U251MG cells, either untreated or treated with TMZ, were used to treat their respective parent cell lines. To further assess potential cross-cell line effects, U87MG cells were incubated with U251MG-derived EVs and U251MG cells with U87MG-derived EVs (see scheme in Figure 3D).

Effects of EVs derived from TMZ-treated U87MG and U251MG cells on the migration of recipient GBM cells

It is important to confirm the internalisation of EVs and assess their uptake rate before investigating their effects on recipient cells. Following the procedure outlined in Figure 3D, U87MG and U251MG cells were incubated with PKH26-labelled GBM-derived EVs for 1, 3, and 24 h. Internalisation was evaluated using fluorescence microscopy. All experimental groups generally showed maximum uptake 24 h after treatment. EVs from untreated GBM cells showed the highest internalization compared with those from TMZ-treated cells [Figure 3E and F, Supplementary Figure 3]. In line with the proteomic analysis, we evaluated GBM cell migratory activity using a wound-healing assay to assess their functional response to EV treatments. As shown in Figure 3C, the cell migration cluster was found to be significantly activated based on the protein cargo of EVs derived from U87MG and U251MG cells after TMZ treatment compared with untreated EVs (z-score values were 6.833 and 2.862, respectively, for U87MG- and U251MG-derived EVs). In addition, 116/176 proteins in U87MG-derived EVs were involved in the cell migration function and were significantly modulated in EVs isolated from TMZ-treated cells, compared to 47/56 proteins in U251MG-derived EVs under the same treatment conditions. As shown in the mechanistic networks of Figure 4A, the majority of these proteins were quantified as unique proteins in EVs derived from U87MG cells treated with TMZ (shown as red shapes in the functional network). Figures 4B and C show the migratory activity of donor GBM cells. TMZ treatment alone did not affect the migratory activity of U87MG cells, but it slowed the migratory activity of U251MG cells over longer periods [Figure 4B and C].

Treatment with EVs derived from U87MG cells, whether exposed to TMZ or not, promoted the migratory activity of recipient U87MG cells as early as 3 h after the scratch was made [Figure 4D (top panel)]. In contrast, only EVs isolated from TMZ-treated U87MG cells enhanced migration in recipient U251MG cells

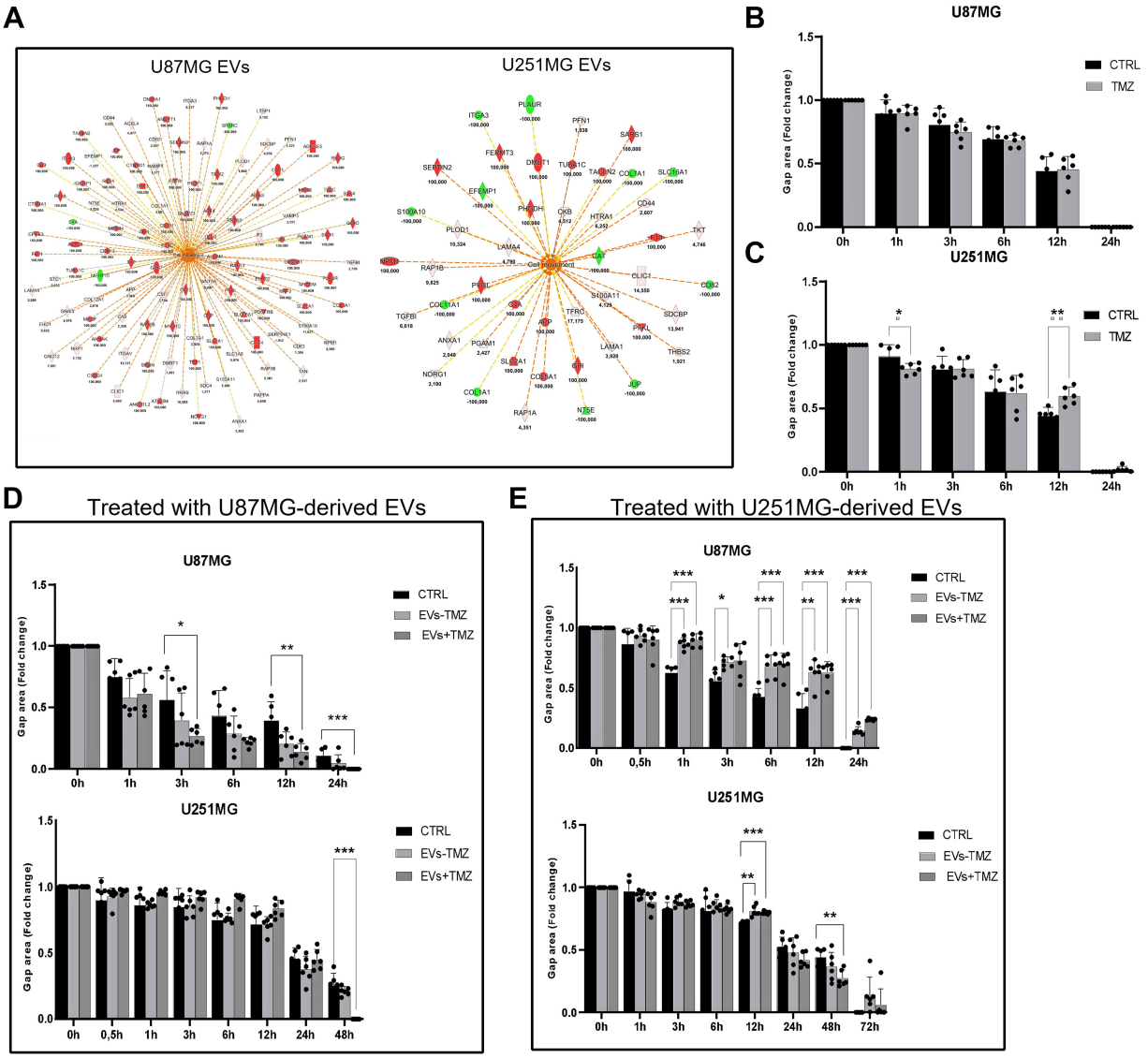


Figure 4. The effect of TMZ treatment on GBM-derived EVs and the migratory activity of TMZ-treated and EV-treated recipient GBM cells. (A) Downstream effect analysis of EV protein datasets revealed the predicted activation of the "Cell Movement" biofunction. Orange and blue shapes represent predicted activation or inhibition, respectively. Instead, red and green shapes represent increased or decreased EV-quantified protein measurements, respectively, with expression values reported in the figure (ratio: EVs +TMZ/EVs -TMZ). Continuous lines represent direct relationships, dotted lines represent indirect relationships, whereas grey and yellow lines indicate the non-predicted and inconsistent relationships. Quantitative data graph of wound healing assay in untreated and TMZ-treated U87MG (B) and U251MG (C) cells measured at 0, 1, 3, 6, 12, and 24 h. The gap area at 0 h was set to 1, and the gap area at 1, 3, 6, 12, and 24 h was calculated as a fold change relative to that. Data are presented as mean ± SD of three independent biological replicates ($n = 3$). $^{*}P < 0.05$, $^{**}P < 0.01$, $^{***}P < 0.001$ *vs.* control (Student's *t*-test); Quantitative data of wound healing assay of U87MG and U251MG cells treated with EVs from untreated (EVs -TMZ) and TMZ-treated (EVs +TMZ) U87MG (D) and U251MG (E) cells measured at 0, 1, 3, 6, 12, and 24 h for both cell lines, and additionally at 48 and 72 h for U251MG cells. The gap area at 0 h was normalized to 1 for each experimental group, and gap areas at later time points, until gap closure, were expressed as a fold change relative to 0 h. Data are presented as mean ± SD of three independent biological replicates ($n = 3$). $^{*}P < 0.05$, $^{**}P < 0.01$, $^{***}P < 0.001$ *vs.* control (Student's *t*-test). Representative bright-field images of the scratch are shown in Supplementary Figure 4. EVs: Extracellular vesicles; GBM: glioblastoma; SD: standard deviation; TMZ: temozolomide.

at later time points, with a significant effect observed at 48 h post-scratch [Figure 4D (bottom panel)]. When U87MG cells were treated with EVs derived from both untreated and TMZ-treated U251MG cells, reduced gap closure was observed as early as 1 h post-scratch, indicating reduced migratory activity [Figure 4E (top panel)]. Conversely, U251MG-derived EVs stimulated migration in recipient U251MG cells, but only at later time points, becoming evident at 48 h [Figure 4E (bottom panel)].

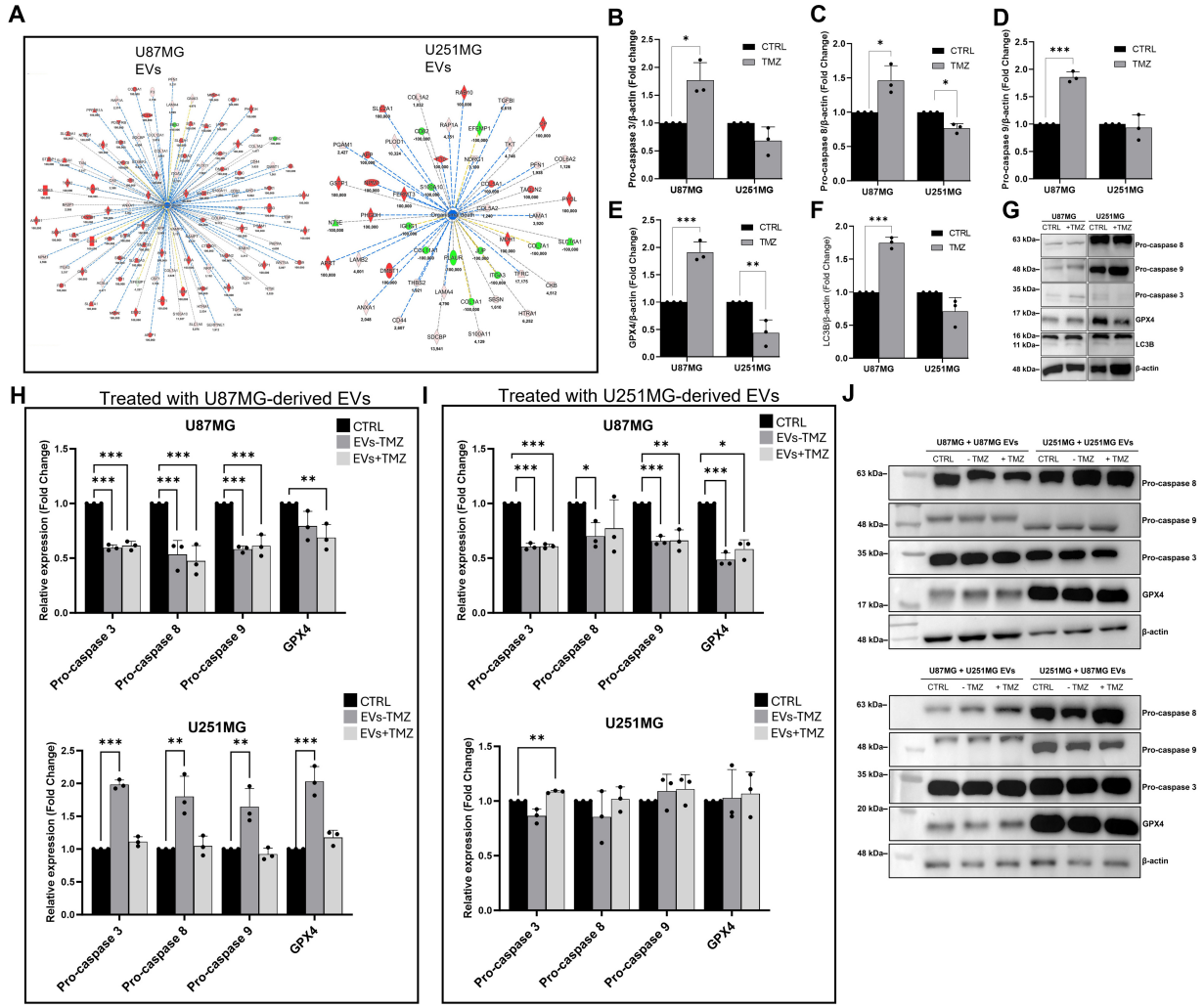


Figure 5. Effect of TMZ treatment on GBM-derived EVs and the expression of cell death- and stress-associated markers in TMZ-treated and EV-treated recipient GBM cells. (A) Downstream effect analysis of EV protein datasets revealed the inhibition of "Organismal Death" biofunction. Orange and blue shapes represent predicted activation or inhibition, respectively. Instead, red and green shapes represent increases or decreases in measurements of EV proteins, respectively, whose expression values are reported in the figure (ratio: EVs +TMZ/ EVs -TMZ). Continuous lines represent direct relationships, dotted ones represent indirect relationships, whereas grey and yellow lines indicate the non-predicted and inconsistent relationships. Expression levels of pro-caspase 3 (B), pro-caspase 8 (C), pro-caspase 9 (D), GPX4 (E), LC3B (F), and relative representative blots (G) of U87MG and U251MG cells untreated (control, CTRL) and TMZ-treated (TMZ) as determined by Western blot analysis; expression levels of pro-caspase 3, pro-caspase 8, pro-caspase 9, and GPX4 in untreated (CTRL) U87MG and U251MG and treated with EVs isolated from untreated (EVs -TMZ) and TMZ-treated (EVs +TMZ) U87MG (H) and U251MG (I) cells and relative representative blot acquisitions (J); Data are normalized to β-actin and expressed as fold change compared to the CTRL group. Statistically significant differences between groups were determined using one-way ANOVA followed by Tukey's post hoc test ***$P < 0.001$. Data are presented as mean ± SD of three independent biological replicates ($n = 3$). Original and uncropped blots are reported in Supplementary Figure 5. ANOVA: Analysis of variance; CTRL: control; EVs: extracellular vesicles; GBM: glioblastoma; GPX4: glutathione peroxidase 4; LC3B: microtubule-associated protein 1 light chain beta; SD: standard deviation; TMZ: temozolomide.

Effects of TMZ-treated U87MG- and U251MG-derived EVs on cell death in recipient GBM cells

The proteomic analysis of EVs revealed that "Organismal Death" was significantly inhibited based on the EV protein cargo of both GBM cell lines when they were treated with TMZ (z-score equal to -7.218 and -3.33 for U87MG- and U251MG-derived EVs, respectively). In particular, as reported in the networks of Figure 5A, U87MG-derived EVs were packaged with proteins that were mainly activated during TMZ treatment, in contrast to U251MG-derived EVs (see red shapes). Western blot analysis revealed an increased expression of key cell death-related markers, including pro-caspase-3, -8, and -9, GPX4 (ferroptosis marker), and microtubule-associated protein 1 LC3B (autophagic marker) in U87MG cells following TMZ treatment [Figure 5B-G]. Conversely, in U251MG cells treated with TMZ, a decrease in the expression of the same markers was observed [Figure 5B-G].

When U87MG cells were treated with EVs isolated from either U87MG or U251MG cells, regardless of whether the parental cells were treated, levels of pro-caspase-3, -8, -9, and GPX4 decreased [Figure 5H-J]. A significant upregulation of these markers was detected in U251MG cells following exposure to EVs isolated from untreated U87MG cells [Figure 5H (bottom panel)]. In contrast, when U251MG cells were treated with EVs derived from U251MG cells, regardless of TMZ treatment, no significant changes were detected in the levels of pro-caspase-3, -8, -9, or GPX4, with the only exception of an increase in pro-caspase-3 levels following incubation with EVs derived from TMZ-treated U251MG cells [Figure 5I (bottom panel) and J]. The evidence shown demonstrates that GBM cells release diverse populations of EVs, whose characteristics and effects are influenced by TMZ treatment.

Effects of U87MG- and U251MG-derived EVs on BMDCs and BV-2 microglial cells

Proteomics results highlighted a consistent set of EV-associated proteins involved in strong immune activation following TMZ treatment [Figure 3C]. The functional networks shown in Figure 6A predicted significant activation of the "Inflammatory Response" (z-score = 3.825) and "Immune Response of Cells" (z-score = 2.077) biofunctions in U87MG-derived EVs isolated from TMZ-treated cells; in contrast, the protein cargo of U251MG-derived EVs in TMZ-treated condition predicted only a slight, non-significant activation of the "Immune Response of Cells" biofunction (z-score = 1.335). In this regard, the effects of GBM-derived EVs on the activation of BV-2 microglial cells and BMDCs were investigated. These antigen-presenting cells are components of the TME and play a crucial role in the immune response against GBM. For BV-2 activation and polarization, no effects on CD80 and CD206 protein expression were observed after exposure to GBM-derived EVs [Figure 6B and Supplementary Figure 6]. Conversely, analysis of the transcript levels of the pro-inflammatory cytokine IL-1β [Figure 6C] showed a significant increase after treatment with EVs from both untreated and TMZ-treated GBM cells. The polarization of BV-2 cells appeared to be partial, as the expression of IL-1β increased, whereas no upregulation of CD80 was observed. No differences were determined in the mRNA levels of the anti-inflammatory cytokine IL-10 [Figure 6D].

As shown in Figure 6E, PKH26-labelled EVs from both untreated and TMZ-treated U87MG and U251MG cells were rapidly internalised by BMDCs just 30 min after exposure. Specific maturation/activation markers for BMDCs[40] (CD80, CD86, and MHCII) were evaluated using flow cytometry [Figure 6F-H and Supplementary Figure 7]. Exposure to EVs from both TMZ-treated U87MG and U251MG cells increased expression of CD80, CD86, and MHCII markers in BMDCs compared to EVs derived from untreated GBM cells [Figure 6F-H and Supplementary Figure 7].

DISCUSSION

This work represents a contribution to the broader scientific interest in identifying new therapeutic strategies based on a detailed understanding of GBM biology. For this reason, the present research has focused on the role of GBM-derived EVs, with the aim of understanding their function and potential applications within the brain tumour. Specifically, the role of GBM-derived EVs as signalling mediators of the TME among various GBM cells, BMDCs, and BV-2 cells was investigated. Although this study is based on *in vitro* experiments, the experimental design was intended to capture aspects of the heterogeneity of tumours *in vivo* and to investigate the effects of TMZ, the standard-of-care chemotherapeutic agent in GBM. The use of four GBM cell lines (U87MG, U251MG, U373MG, and T98G) with differences in proliferation, morphology, and response to treatments such as radiation and TMZ was aimed to reflect the cellular heterogeneity found in glioblastoma tumours[41,42]. For example, the U87MG cell line, characterized by neuronal-like morphology, is more sensitive to TMZ, while T98G, which has fibroblast-like morphology, is more resistant to TMZ and is recommended for studying glycolysis. U251MG and U373MG cell lines have intermediate characteristics, with U373MG showing some similarity to U251MG in certain metabolic aspects[29]. Furthermore, the cell lines differ in the expression of O6-methylguanine-DNA methyltransferase (MGMT), a DNA repair enzyme

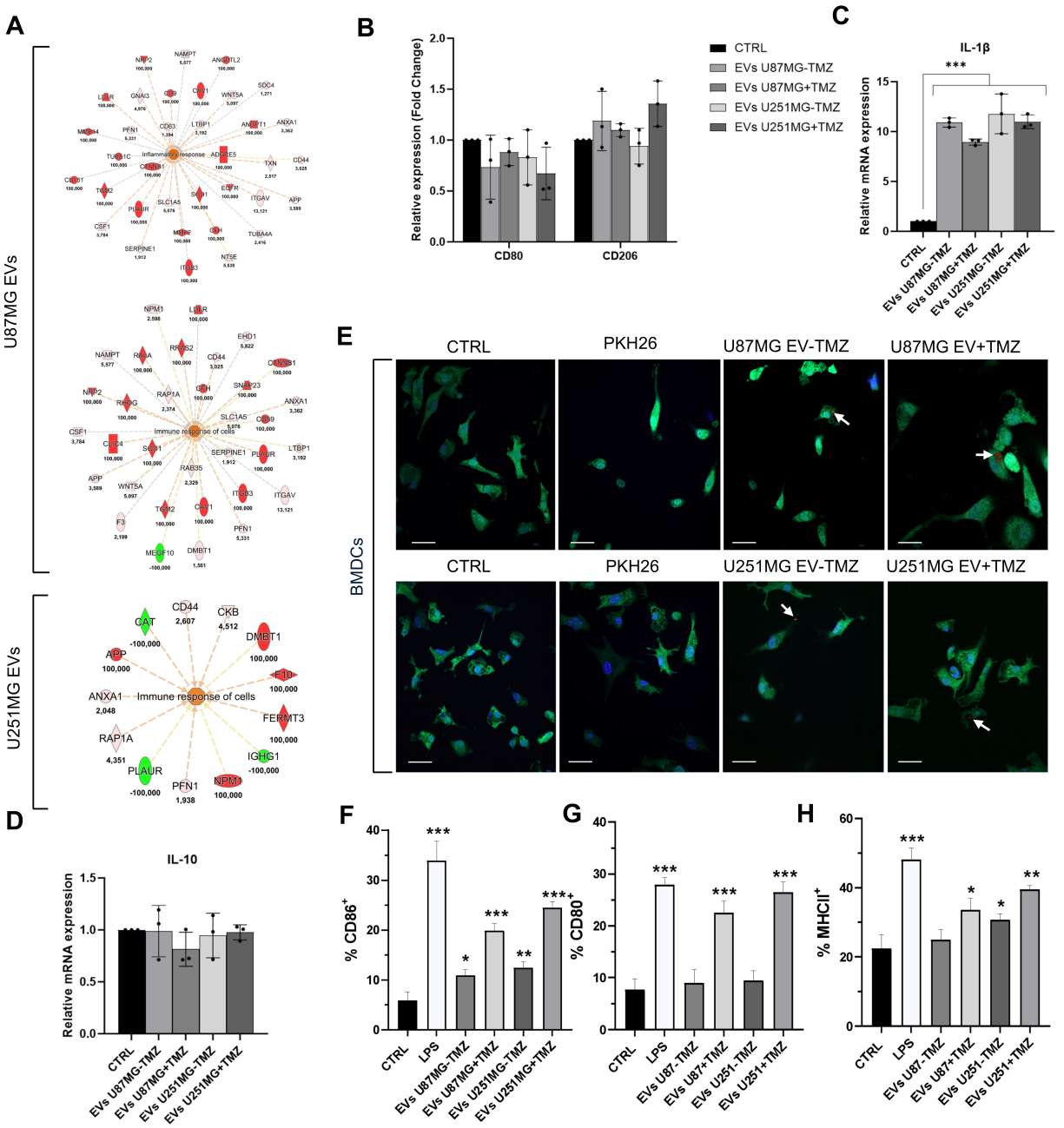


Figure 6. Effects of GBM-derived EVs on maturation/activation of BMDCs and BV-2 microglial cells. (A) Downstream effects analysis of EV protein datasets revealed the predicted activation of the "Immune Response of Cells" biofunction. Orange and blue shapes represent predicted activation or inhibition, respectively. Instead, red and green shapes represent increased or decreased measurements of EV-quantified proteins, respectively, whose expression values are reported in the figure (ratio: EVs +TMZ/ EVs -TMZ). Continuous lines represent direct relationships, dotted lines represent indirect relationships, and grey and yellow lines indicate non-predicted and inconsistent relationships. (B) Expression of CD80 and CD206 in BV-2 cells treated with GBM-derived EVs detected by Western blot analysis. Data are normalized to β-actin and expressed as fold change compared to the untreated (CTRL) group. Data are presented as mean ± SD of three independent biological replicates ($n = 3$). Original uncropped blots are reported in Supplementary Figure 6. Relative mRNA expression levels of IL-1β (C) and IL-10 (D) in BV-2 cells treated with EVs derived from untreated and TMZ-treated U87MG and U251MG cells. Data are expressed as fold change compared to control (CTRL, untreated) and normalized to the housekeeping gene Tbp. Statistically significant differences between groups were determined using one-way ANOVA followed by Tukey's post hoc test $^{***}P < 0.001$. Data are presented as mean ± SD of three independent biological replicates ($n = 3$). (E) Microscopy fluorescence images showing the uptake of PKH26-labelled EVs derived from untreated (EVs -TMZ) and TMZ-treated (EVs +TMZ) U87MG and U251MG cells in recipient BMDCs after 30 min of incubation. Internalized EVs are indicated by white arrows (scale bar: 20 μm); CD86 (F), CD80 (G), and MHCII (H) expression on BMDC surfaces was assessed by flow cytometry. LPS-treated BMDCs were used as positive controls. Statistically significant differences between groups were determined using one-way ANOVA followed by Tukey's post hoc test, $^{*}P < 0.05$, $^{**}P < 0.01$, $^{***}P < 0.001$. Data are presented as the mean ± SD of three independent biological replicates ($n = 3$). ANOVA: Analysis of variance; BMDCs: bone marrow-derived dendritic cells; CD80: cluster of differentiation 80; CD86: cluster of differentiation 86; CD206: cluster of differentiation 206; CTRL: control; EVs: extracellular vesicles; GBM: glioblastoma; IL-1β: interleukin-1 beta; IL-10: interleukin-10; LPS: lipopolysaccharide; MHCII: major histocompatibility complex class II; PKH26: red fluorescent cell membrane dye; SD: standard deviation; TMZ: temozolomide; Tbp: TATA-box binding protein.

that promotes resistance of cancer cells to alkylating agents, including TMZ. U87MG, U373MG, and U251MG are generally characterized by low or absent MGMT expression and methylated MGMT promoters, whereas T98G exhibits high MGMT expression and an unmethylated MGMT promoter[43-45]. Thus, T98G is considered more resistant to TMZ than the other GBM cell lines, although additional molecular mechanisms contribute to TMZ sensitivity[46].

Evaluating the dose- and time-dependent responses of the four GBM cell lines to TMZ enabled us to categorise them according to their sensitivity to the drug and determine suitable treatment conditions for subsequent experiments, which revealed TMZ-induced changes in the amount and characteristics of released EVs. The potential pro- or anti-tumorigenic effects of EVs in the TME were investigated using a comparative approach, evaluating EVs derived from untreated or TMZ-treated GBM cells. Indeed, this study reported that GBM cells differ in their response to TMZ treatment in terms of the expression of cell death-related markers, migratory rate, and EV production. Notably, this study focused on investigating the potential pro- or anti-tumorigenic role of EVs during TMZ treatment in recipient GBM cells *in vitro*. However, it did not explore the molecular mechanisms underlying drug resistance in depth. Instead, it aimed to elucidate whether EVs play a role in shaping the tumour response to chemotherapy. The first mandatory step for the correct study of EVs and their role is to isolate and thoroughly characterise them following the MISEV guidelines[19]. As isolating EVs is challenging, it is crucial to select the most appropriate isolation method and confirm the presence of MVBs and surface budding throughout the cell. This was done to extensively characterise GBM-derived EVs, assess their heterogeneity, and establish whether TMZ interfered with their production. In this work, of the various methods for concentrating and purifying EVs, such as ultracentrifugation (UC), UF, SEC, polymer-based precipitation, and immunoaffinity-based precipitation, the UF/SEC combination was selected because it produces purer EV fractions with a higher yield and is more suitable for functional studies[47-49]. As expected, significant differences were observed in the number, size, and shape of EVs produced by the four GBM cell lines, without and under TMZ administration. The absence of non-EV particles and other detectable contaminants, as confirmed by cryo-EM analysis, indicates that the observed changes in EV size and concentration most likely reflect TMZ-induced cellular alterations rather than contamination of EV-enriched fractions[33]. In fact, as widely reported in the literature[50], the EVs are modulated by various factors. The observed heterogeneity of EVs in terms of size and quantity reflected the GBM cell line of origin and was also evident in the differential responses to TMZ treatment. Following treatment with TMZ, the quantity and mean size of produced EVs generally increased. Our findings align with those of André-Grégoire *et al.*, who observed an increase in released EVs in GBM stem-like cells following TMZ exposure[51]. Other observations are in agreement with the findings reported in the present study. The number of EVs can increase following chemotherapy[52,53]. Whether the number of EVs released increases or decreases following TMZ treatment seems to depend on the GBM cell lines and treatment conditions[54,55].

The quality of isolation was validated through various standardised procedures, such as NTA, TEM, cryo-EM, and AFM. The technical characteristics of the different instruments may explain the slight differences in size found with the various procedures used. Notably, further sizing of EVs by AFM corroborates the TEM data, providing a significantly higher statistical value[35]. TMZ treatment affected several characteristics of EVs across all GBM cell lines, although the changes were cell line specific. Changes in EVs and the extent of modification are related to quantity, morphology, size, and, for budding vesicles only, distribution on the cell surface. Cryo-EM imaging revealed that most released EVs are surrounded by a single lipid bilayer; however, a subset of multilayered EVs was identified in all four GBM cell lines, and their relative percentage increased after TMZ treatment (except for U373MG)[33]. Advanced AFM revealed that TMZ treatment induced

extensive modulation of budding vesicle distribution, concentrating them in areas close to the nucleus. Information about the topographical distribution of budding vesicles on the cell surface is still scarce. However, research in this area could reveal new insights into the trafficking of EVs, both intracellularly and in terms of their location of release on the cell surface[56,57]. Indeed, AFM revealed a differential profile of plasma membrane budding between physiological and drug-treated conditions, indicating a potential relationship between mechanical characteristics and functional role[35]. The mechanical characteristics of the plasma membrane have recently been considered as possible therapeutic targets[58,59]. Cryo-EM analysis of EVs isolated from the GBM cell lines used in this study, either untreated or TMZ-treated, demonstrated that only a small proportion of GBM-derived EVs exhibited a protein corona[33]. The use of EV-depleted FBS-supplemented DMEM for EV isolation from GBM cell-conditioned medium may explain the low frequency of corona-coated EVs. UC-based depletion of FBS partially removes not only bovine EVs but also a proportion of protein complexes and lipoproteins, potentially reducing corona formation[60]. Purification of EVs by SEC efficiently removes unbound proteins while largely preserving proteins associated with the EV surface[23]. Indeed, protein corona is retained on EVs isolated by SEC and can be modified by high-salt washings[61]. Based on our cryo-EM observations, we propose that the majority of proteins identified in analysis of GBM-derived EVs represent intrinsic proteins rather than proteins associated with the EV surface. Although multiple studies have characterized the proteome of GBM-derived EVs, there is a lack of research on corona-associated proteins[62-64].

As more data becomes available, it is becoming increasingly clear that the formation of EVs is much more diverse and complex than previously described. Currently, research is adding other types and pathways of EVs to the two main pathways for the formation of exosomes and ectosomes[65-67].

EVs mediate cellular signalling through their cargo, whose composition depends on numerous factors, including cell type and stress conditions, which explains their high heterogeneity. Furthermore, the effects of the chemotherapeutic agent TMZ on the full protein cargo composition of GBM-derived EVs have never been characterized. Thus, in-depth investigation into the role of EVs in maintaining a specific microenvironment and promoting tumorigenicity requires omics characterisation of their cargo. In a previous study, treatment of GBM (LN18 and U87 cells) with the anti-angiogenic drug bevacizumab and subsequent analysis of EVs showed some similarities with EVs from TMZ-treated cells, such as an upregulation of Annexin A2, which is a marker of angiogenesis and tumour progression[55].

It should be noted that the proteomic data of this study are based on comparisons between different GBM cell lines, as well as within individual lines, between the presence or absence of chemotherapeutic drugs. As a general response, proteomic analysis of EVs produced by different GBM cell lines revealed that TMZ treatment modifies both the molecular content and the quantity of proteins. Significantly upregulated proteins were identified and quantified in EVs derived from GBM cell lines treated with TMZ compared to baseline conditions [Figure 3A and B], highlighting that they were mainly involved in the modulation of key functions of tumorigenic processes, such as migratory activity, cell death, and immune system function (see Figure 3C and the mechanistic networks in Figures 4-6). In this regard, the ability of EVs to transfer functional signals to other GBM cells present in the tumour was verified by incubating them with EVs isolated from the various experimental groups, namely U87MG and U251MG, as illustrated in the scheme of Figure 3D.

Effective internalisation of EVs by recipient cells is required for EV-mediated communication. EV uptake, whether derived from non-TMZ-treated or TMZ-treated cells, was time-dependent for both U87MG and U251MG cell lines. However, even if common differences have been found among all the analysed functions, once again the profound heterogeneity among GBM cells was highlighted. Changes in cells following

treatment with TMZ do not always correspond to those observed in the EVs they produce. In some cases, the EVs themselves appear different. Could these differences be used as disease markers? Furthermore, in some cases, the responses elicited by EVs in recipient cells are the opposite of those induced by TMZ treatment in donor cells.

The reasons for this behaviour require extensive study and cannot be explained by mere speculation. However, it could be hypothesised that recipient cells respond to the presence of EVs in a way that protects tumour growth. Of even greater interest is the GBM cell-dependent response to the stimulus induced by treatment with the same EVs. Previous studies supported the protumoral effects of GBM-derived EVs. For example, Ma *et al*. showed that GBM stem cell-derived EVs induce radiation resistance and modulate the TME to promote glioma progression[68]. EVs isolated from TMZ-treated U87MG and LN229 cells may play a role in TMZ resistance through an increase in expression of heat shock proteins (HSPs)[69].

In short, U87MG recipient cells appeared to be more sensitive to EV treatments than U251MG cells. Nevertheless, only EVs derived from U87MG cells influenced the expression of cell death-related markers in both cell lines. For example, the variations in cell death-related proteins observed in EVs derived from U87MG cells did not correlate with the changes observed in the parental cells. The upregulation of pro-caspase-3 has been reported to correlate with a higher tumour grade and poorer prognosis in patients[70]. Moreover, in GBM, an increased expression of caspase-8 in non-apoptotic contexts contributes to tumour progression by promoting angiogenesis and resistance to chemotherapy through nuclear factor kappa B (NF-κB) activation[71]. A comparable response was observed for migratory activity. Interestingly, the biological effects of TMZ on donor cells in terms of migratory activity did not correlate with variations in the expression of migration-related proteins in EVs. This suggests that EVs contain proteins associated with migration that do not accurately reflect the functional state of the donor cells. The type of response induced may be influenced by differences in recipient cells, such as their functional status and the receptors they express.

DCs play a crucial role in the immune response against GBM as professional antigen-presenting cells responsible for initiating and regulating T cell-mediated immunity[72]. However, in the context of GBM, the immunosuppressive TME can impair DC maturation and function, resulting in reduced antigen presentation and diminished anti-tumour responses[73]. Our data showed an increase in maturation and activation markers in BMDCs in response to EVs isolated from TMZ-treated cells, but not to EVs derived from the untreated cells. This highlights the EV-mediated immunosuppressive effect exerted by GBM, which is diminished following TMZ treatment. As a targeted immunotherapeutic strategy against GBM, the immunomodulatory effects of GBM-derived EVs on BMDCs warrant deeper investigation, with the aim of identifying novel potential therapeutic targets.

Some limitations of this study should be acknowledged. The use of established cell lines instead of patient-derived cells may not fully reflect the molecular heterogeneity of GBM. It should be noted that, in this study, murine BV-2 microglial cells and murine BMDCs were treated with EVs isolated from human GBM cell lines. Although species-specific differences may influence cellular responses, models utilizing human cell-derived EVs and murine recipient cells are widely used in research, including recent studies on human GBM-derived EVs and murine immune cells[74-77]. Moreover, the fundamental mechanisms of EV uptake and intracellular trafficking are conserved across diverse cell types[78]. The immunotoxicity of human EVs should be carefully considered, particularly in preclinical studies and experiments using rodent models. Several studies have reported that human EVs exhibit low cytotoxicity and immunogenicity in rodent recipients, while emphasizing that these properties depend on the cellular origin and composition of EVs[79]. Future studies with primary human immune cells, patient-derived GBM models, and *in vivo* validation will be important to confirm and expand these findings.

In conclusion, our data show that chemotherapy actively reshapes the EV landscape in GBM: TMZ altered the concentration, morphology, and protein cargo of GBM-derived EVs in a cell line-specific manner, changing the abundance of proteins linked to migration, cell death, and immune pathways. These EVs were efficiently internalized by recipient GBM and immune cells, driving variable changes in migratory activity, death-marker expression, and immune activation. While the underlying molecular mechanisms remain to be fully defined, these findings expand current knowledge of how chemotherapy shapes EV-mediated signalling in GBM and identify EV-associated features as candidate biomarkers of therapeutic response.

DECLARATIONS

Acknowledgments

The authors sincerely thank Greet De Smet for her invaluable technical assistance in the CDIT laboratory. The authors gratefully acknowledge Frédéric Clement, Maarten Verdonckt, and Sophie Vermaut of the Core Flow Cytometry (BOF/COR/2022/009) at Ghent University (Belgium) for the use and/or support of the BD LSR Fortessa flow cytometer.

This manuscript is dedicated to the memory of Professor Dmitry V. Krysko (Ghent University), whose untimely passing is a great loss to the scientific community. We gratefully acknowledge his mentorship and generosity in hosting Dr. Diana Vardanyan in his research team at Ghent University during her PhD, an experience that significantly contributed to her scientific development.

Authors' contributions

Were involved in the experiments of the study and drafted the manuscript: Vardanyan D, Karimova M
BMDCs isolation and flow cytometry analysis: Efimova I
NTA analysis: Fratini F
AFM analysis: Dinarelli S
Mass spectrometry analysis and proteomic data interpretation: Cufaro MC, Del Boccio P
Cryo-EM imaging: Alfieri A, Zuccotti M
Conceptualization, supervision and drafting of the manuscript: Tacconi S, Dini L
Figures preparation: Tacconi S
Drafting, editing and revision of the final version of the manuscript: Zuccotti M, Del Boccio P, Chieppa M, Krysko DV, Dini L, Tacconi S

Availability of data and materials

All data from this article are available upon request. Proteomics data have been deposited in ProteomeXchange/PRIDE under accession number PXD070357.

AI and AI-assisted tools statement

During the preparation of this manuscript, the AI tool DeepL Translator (Next-Generation Language Model, released 2024-07-17) was used solely for language editing. In addition, the AI tool ChatGPT (GPT-5.2, released 2025-11-11) was used solely to generate part of the Graphical Abstract and Figure 3D. The tools did not influence the study design, data collection, analysis, interpretation, or the scientific content of the work. All authors take full responsibility for the accuracy, integrity, and final content of the manuscript.

Financial support and sponsorship

This work was supported by CHIEPPA.AIRC_IG2025_ID31970 - Progetto IG, Rif. 31970 - Iron-Sequestration as Adjuvant Against CRC Development; Prof. Chieppa M. The CDIT Laboratory was supported by the Flanders Research Foundation (FWO) and the Belgian National Fund for Scientific Research (F.R.S.-FNRS) under the Excellence of Science (EOS) program (40007488), Special Research Fund (BOF) grants from Ghent University (BOF/IOP/2022/033, BOF23/GOA/029).

Conflicts of interest

All authors declared that there are no conflicts of interest.

Ethical approval and consent to participate

The experiments were conducted in accordance with the ethical guidelines of the local ethics committee of the Faculty of Medicine and Health Sciences of Ghent University (Belgium; accreditation number LA1400080, project ECD 20/06aanp).

Consent for publication

Not applicable.

Copyright

© The Author(s) 2026.

Supplementary Materials

Supplementary Materials

REFERENCES

1. Sipos D, Raposa BL, Freihat O, et al. Glioblastoma: clinical presentation, multidisciplinary management, and long-term outcomes. *Cancers.* 2025;17:146. DOI PubMed PMC
2. Seker-Polat F, Pinarbasi Degirmenci N, Solaroglu I, Bagci-Onder T. Tumor cell infiltration into the brain in glioblastoma: from mechanisms to clinical perspectives. *Cancers.* 2022;14:443. DOI PubMed PMC
3. Narsinh KH, Perez E, Haddad AF, et al. Strategies to improve drug delivery across the blood-brain barrier for glioblastoma. *Curr Neurol Neurosci Rep.* 2024;24:123-39. DOI PubMed PMC
4. Stupp R, Weller M, Belanger K, et al. Radiotherapy plus concomitant and adjuvant temozolomide for glioblastoma. *N Engl J Med.* 2005;352:987-96. DOI PubMed
5. Parsons DW, Jones S, Zhang X, et al. An integrated genomic analysis of human glioblastoma multiforme. *Science.* 2008;321:1807-12. DOI PubMed PMC
6. Yan H, Parsons DW, Jin G, et al. IDH1 and IDH2 mutations in gliomas. *N Engl J Med.* 2009;360:2248-9. DOI PubMed
7. Verhaak RG, Hoadley KA, Purdom E, et al. ; Cancer Genome Atlas Research Network. Integrated genomic analysis identifies clinically relevant subtypes of glioblastoma characterized by abnormalities in PDGFRA, IDH1, EGFR, and NF1. *Cancer Cell.* 2010;17:98-110. DOI PubMed PMC
8. Mishchenko TA, Turubanova VD, Gorshkova EN, Krysko O, Vedunova MV, Krysko DV. Glioma: bridging the tumor microenvironment, patient immune profiles and novel personalized immunotherapy. *Front Immunol.* 2023;14:1299064. DOI PubMed PMC
9. Sharma P, Aaroe A, Liang J, Puduvalli VK. Tumor microenvironment in glioblastoma: Current and emerging concepts. *Neurooncol Adv.* 2023;5:vdad009. DOI PubMed PMC
10. Manini I, Caponnetto F, Bartolini A, et al. Role of microenvironment in glioma invasion: what we learned from in vitro models. *Int J Mol Sci.* 2018;19:147. DOI PubMed PMC
11. White J, White MPJ, Wickremesekera A, Peng L, Gray C. The tumour microenvironment, treatment resistance and recurrence in glioblastoma. *J Transl Med.* 2024;22:540. DOI PubMed PMC
12. Yekula A, Yekula A, Muralidharan K, Kang K, Carter BS, Balaj L. Extracellular vesicles in glioblastoma tumor microenvironment. *Front Immunol.* 2019;10:3137. DOI PubMed PMC
13. Clancy JW, D'Souza-Schorey C. Tumor-derived extracellular vesicles: multifunctional entities in the tumor microenvironment. *Annu Rev Pathol.* 2023;18:205-29. DOI PubMed PMC
14. Xin W, Pan Y, Wei W, et al. Preconditioned extracellular vesicles from hypoxic microglia reduce poststroke AQP4 depolarization, disturbed cerebrospinal fluid flow, astrogliosis, and neuroinflammation. *Theranostics.* 2023;13:4197-216. DOI PubMed PMC
15. Bhavsar V, Sahu A, Taware R. Stress-induced extracellular vesicles: insight into their altered proteomic composition and probable physiological role in cancer. *Mol Cell Biochem.* 2025;480:2025-41. DOI PubMed
16. Xiang H, Bao C, Chen Q, et al. Extracellular vesicles (EVs)' journey in recipient cells: from recognition to cargo release. *J Zhejiang Univ Sci B.* 2024;25:633-55. DOI PubMed PMC
17. Dusoswa SA, Horrevorts SK, Ambrosini M, et al. Glycan modification of glioblastoma-derived extracellular vesicles enhances receptor-mediated targeting of dendritic cells. *J Extracell Vesicles.* 2019;8:1648995. DOI PubMed PMC

18. Cifola I, Fratini F, Cardinali B, et al. miRNome and proteome profiling of small extracellular vesicles secreted by human glioblastoma cell lines and primary cancer stem cells. *Biomedicines.* 2022;10:1886. DOI PubMed PMC
19. Welsh JA, Goberdhan DCI, O'Driscoll L, et al. ; MISEV Consortium. Minimal information for studies of extracellular vesicles (MISEV2023): from basic to advanced approaches. *J Extracell Vesicles.* 2024;13:e12404. DOI PubMed PMC
20. Kang T, Atukorala I, Mathivanan S. Biogenesis of extracellular vesicles. *Subcell Biochem.* 2021;97:19-43. DOI PubMed
21. Musicò A, Zendrini A, Reyes SG, et al. Extracellular vesicles of different cellular origin feature distinct biomolecular corona dynamics. *Nanoscale Horiz.* 2024;10:104-12. DOI PubMed
22. Heidarzadeh M, Zarebkohan A, Rahbarghazi R, Sokullu E. Protein corona and exosomes: new challenges and prospects. *Cell Commun Signal.* 2023;21:64. DOI PubMed PMC
23. Tóth EÁ, Turiák L, Visnovitz T, et al. Formation of a protein corona on the surface of extracellular vesicles in blood plasma. *J Extracell Vesicles.* 2021;10:e12140. DOI PubMed PMC
24. Mishchenko TA, Olajide OJ, Gorshkova EN, Vedunova MV, Krysko DV. Regulated cell death modalities: breaking resistance of temozolomide glioblastoma therapy. *Trends Cancer.* 2025;11:430-2. DOI PubMed
25. Keklikoglou I, Cianciaruso C, Güç E, et al. Chemotherapy elicits pro-metastatic extracellular vesicles in breast cancer models. *Nat Cell Biol.* 2019;21:190-202. DOI PubMed PMC
26. Wang X, Qiao D, Chen L, et al. Chemotherapeutic drugs stimulate the release and recycling of extracellular vesicles to assist cancer cells in developing an urgent chemoresistance. *Mol Cancer.* 2019;18:182. DOI PubMed PMC
27. Wang Q, Hu X, Hu B, et al. Tumor evolution of glioma-intrinsic gene expression subtype associates with immunological changes in the microenvironment. *Cancer Cell.* 2017;32:42-56.e6. DOI PubMed PMC
28. Schnöller LE, Piehlmaier D, Weber P, et al. Systematic in vitro analysis of therapy resistance in glioblastoma cell lines by integration of clonogenic survival data with multi-level molecular data. *Radiat Oncol.* 2023;18:51. DOI PubMed PMC
29. Arthurs AL, Keating DJ, Stringer BW, Conn SJ. The suitability of glioblastoma cell lines as models for primary glioblastoma cell metabolism. *Cancers.* 2020;12:3722. DOI PubMed PMC
30. Vedunova M, Turubanova V, Vershinina O, et al. DC vaccines loaded with glioma cells killed by photodynamic therapy induce Th17 anti-tumor immunity and provide a four-gene signature for glioma prognosis. *Cell Death Dis.* 2022;13:1062. DOI PubMed PMC
31. Sladowski D, Steer SJ, Clothier RH, Balls M. An improved MTT assay. *J Immunol Methods.* 1993;157:203-7. DOI PubMed
32. Böing AN, van der Pol E, Grootemaat AE, Coumans FA, Sturk A, Nieuwland R. Single-step isolation of extracellular vesicles by size-exclusion chromatography. *J Extracell Vesicles.* 2014;3:23430. DOI PubMed PMC
33. Karimova M, Ponziani G, Vardanyan D, et al. Cryogenic electron microscopy of extracellular vesicles from temozolomide-treated glioblastoma cells reveals great morphological heterogeneity. *Nanomaterials.* 2026;16:685. DOI PubMed PMC
34. Sbarigia C, Tacconi S, Mura F, Rossi M, Dinarelli S, Dini L. High-resolution atomic force microscopy as a tool for topographical mapping of surface budding. *Front Cell Dev Biol.* 2022;10:975919. DOI PubMed PMC
35. Schneider CA, Rasband WS, Eliceiri KW. NIH Image to ImageJ: 25 years of image analysis. *Nat Methods.* 2012;9:671-5. DOI PubMed PMC
36. Potenza F, Cufaro MC, Di Biase L, et al. Proteomic analysis of marinesco-sjogren syndrome fibroblasts indicates pro-survival metabolic adaptation to SIL1 loss. *Int J Mol Sci.* 2021;22:12449. DOI PubMed PMC
37. Madonna R, Pieragostino D, Cufaro MC, et al. Ponatinib induces vascular toxicity through the Notch-1 signaling pathway. *J Clin Med.* 2020;9:820. DOI PubMed PMC
38. Pieragostino D, Lanzini M, Cicalini I, et al. Tear proteomics reveals the molecular basis of the efficacy of human recombinant nerve growth factor treatment for Neurotrophic Keratopathy. *Sci Rep.* 2022;12:1229. DOI PubMed PMC
39. Perez-Riverol Y, Bandla C, Kundu DJ, et al. The PRIDE database at 20 years: 2025 update. *Nucleic Acids Res.* 2025;53:D543-53. DOI PubMed PMC
40. Mishchenko TA, Balalaeva IV, Turubanova VD, et al. Chapter 8 - gold standard assessment of immunogenic cell death induced by photodynamic therapy: from in vitro to tumor mouse models and anti-cancer vaccination strategies. *Methods Cell Biol.* 2024;183:203-64. DOI PubMed
41. Network TC. Corrigendum: Comprehensive genomic characterization defines human glioblastoma genes and core pathways. *Nature.* 2013;494:506. DOI PubMed
42. Eisenbarth D, Wang YA. Glioblastoma heterogeneity at single cell resolution. *Oncogene.* 2023;42:2155-65. DOI PubMed PMC
43. Jeuken JW, Cornelissen SJ, Vriezen M, et al. MS-MLPA: an attractive alternative laboratory assay for robust, reliable, and semiquantitative detection of MGMT promoter hypermethylation in gliomas. *Lab Invest.* 2007;87:1055-65. DOI PubMed
44. Anan M, Del Maestro RF, Hata N, Fujiki M. O^6 -methylguanine methyltransferase promoter methylation status of glioblastoma cell line clonal population. *Neuropathology.* 2024;44:41-6. DOI PubMed

45. Abe H, Natsumeda M, Okada M, et al. MGMT expression contributes to temozolomide resistance in H3K27M-mutant diffuse midline gliomas. *Front Oncol.* 2019;9:1568. DOI PubMed PMC
46. Pu J, Yuan K, Tao J, et al. Glioblastoma multiforme: an updated overview of temozolomide resistance mechanisms and strategies to overcome resistance. *Discov Oncol.* 2025;16:731. DOI PubMed PMC
47. Mol EA, Goumans MJ, Doevendans PA, Sluijter JPG, Vader P. Higher functionality of extracellular vesicles isolated using size-exclusion chromatography compared to ultracentrifugation. *Nanomedicine.* 2017;13:2061-5. DOI PubMed
48. Paget D, Checa A, Zöhrer B, et al. ; Oxford Acute Myocardial Infarction Study (OxAMI). Comparative and integrated analysis of plasma extracellular vesicle isolation methods in healthy volunteers and patients following myocardial infarction. *J Extracell Biol.* 2022;1:e66. DOI PubMed PMC
49. Grenhas M, Lopes R, Ferreira BV, Barahona F, João C, Carneiro EA. Size-exclusion chromatography: a path to higher yield and reproducibility compared to sucrose cushion ultracentrifugation for extracellular vesicle isolation in multiple myeloma. *Int J Mol Sci.* 2024;25:8496. DOI PubMed PMC
50. Berumen Sánchez G, Bunn KE, Pua HH, Rafat M. Extracellular vesicles: mediators of intercellular communication in tissue injury and disease. *Cell Commun Signal.* 2021;19:104. DOI PubMed PMC
51. André-Grégoire G, Bidère N, Gavard J. Temozolomide affects extracellular vesicles released by glioblastoma cells. *Biochimie.* 2018;155:11-5. DOI PubMed
52. Bandari SK, Purushothaman A, Ramani VC, et al. Chemotherapy induces secretion of exosomes loaded with heparanase that degrades extracellular matrix and impacts tumor and host cell behavior. *Matrix Biol.* 2018;65:104-18. DOI PubMed PMC
53. Ab Razak NS, Ab Mutalib NS, Mohtar MA, Abu N. Impact of chemotherapy on extracellular vesicles: understanding the chemo-EVs. *Front Oncol.* 2019;9:1113. DOI PubMed PMC
54. Garnier D, Meehan B, Kislinger T, et al. Divergent evolution of temozolomide resistance in glioblastoma stem cells is reflected in extracellular vesicles and coupled with radiosensitization. *Neuro Oncol.* 2018;20:236-48. DOI PubMed PMC
55. Simon T, Pinioti S, Schellenberger P, et al. Shedding of bevacizumab in tumour cells-derived extracellular vesicles as a new therapeutic escape mechanism in glioblastoma. *Mol Cancer.* 2018;17:132. DOI PubMed PMC
56. Casado S, Lobo MDVT, Paíno CL. Dynamics of plasma membrane surface related to the release of extracellular vesicles by mesenchymal stem cells in culture. *Sci Rep.* 2017;7:6767. DOI PubMed PMC
57. Mitani F, Hayasaka R, Hirayama A, Oneyama C. SNAP23-mediated perturbation of cholesterol-enriched membrane microdomain promotes extracellular vesicle production in Src-activated cancer cells. *Biol Pharm Bull.* 2022;45:1572-80. DOI PubMed
58. Mukhopadhyay U, Mandal T, Chakraborty M, Sinha B. The plasma membrane and mechanoregulation in cells. *ACS Omega.* 2024;9:21780-97. DOI PubMed PMC
59. Choromańska A, Chwiłkowska A, Kulbacka J, et al. Modifications of plasma membrane organization in cancer cells for targeted therapy. *Molecules.* 2021;26:1850. DOI PubMed PMC
60. Lehrich BM, Liang Y, Fiandaca MS. Foetal bovine serum influence on in vitro extracellular vesicle analyses. *J Extracell Vesicles.* 2021;10:e12061. DOI PubMed PMC
61. Försönits AI, Tóth EÁ, Jezsoviczky S, et al. Improved accessibility of extracellular vesicle surface molecules upon partial removal of the protein corona by high ionic strength. *J Extracell Vesicles.* 2025;14:e70124. DOI PubMed PMC
62. Naryzhny S, Volnitskiy A, Kopylov A, et al. Proteome of glioblastoma-derived exosomes as a source of biomarkers. *Biomedicines.* 2020;8:216. DOI PubMed PMC
63. Hallal S, Russell BP, Wei H, et al. Extracellular vesicles from neurosurgical aspirates identifies chaperonin containing TCP1 subunit 6A as a potential glioblastoma biomarker with prognostic significance. *Proteomics.* 2019;19:e1800157. DOI PubMed
64. Giuliani P, De Simone C, Febo G, et al. Proteomics studies on extracellular vesicles derived from glioblastoma: where do we stand? *Int J Mol Sci* 2024;25:9778. DOI PubMed PMC
65. Ma L, Li Y, Peng J, et al. Discovery of the migrasome, an organelle mediating release of cytoplasmic contents during cell migration. *Cell Res.* 2015;25:24-38. DOI PubMed PMC
66. Minciacchi VR, You S, Spinelli C, et al. Large oncosomes contain distinct protein cargo and represent a separate functional class of tumor-derived extracellular vesicles. *Oncotarget.* 2015;6:11327-41. DOI PubMed PMC
67. Solvik TA, Nguyen TA, Tony Lin YH, et al. Secretory autophagy maintains proteostasis upon lysosome inhibition. *J Cell Biol.* 2022;221:e202110151. DOI PubMed PMC
68. Ma C, Nguyen HPT, Jones JJ, et al. Extracellular vesicles secreted by glioma stem cells are involved in radiation resistance and glioma progression. *Int J Mol Sci.* 2022;23:2770. DOI PubMed PMC
69. Kıyga E, Adıgüzel Z, Önay Uçar E. Temozolomide increases heat shock proteins in extracellular vesicles released from glioblastoma cells. *Mol Biol Rep.* 2022;49:8701-13. DOI PubMed

70. Joshi AD, Botham RC, Schlein LJ, et al. Synergistic and targeted therapy with a procaspase-3 activator and temozolomide extends survival in glioma rodent models and is feasible for the treatment of canine malignant glioma patients. *Oncotarget.* 2017;8:80124-38. DOI PubMed PMC
71. Fianco G, Mongiardi MP, Levi A, et al. Caspase-8 contributes to angiogenesis and chemotherapy resistance in glioblastoma. *Elife.* 2017;6:e22593. DOI PubMed PMC
72. Hu X, Jiang C, Gao Y, Xue X. Human dendritic cell subsets in the glioblastoma-associated microenvironment. *J Neuroimmunol.* 2023;383:578147. DOI PubMed
73. Adhikaree J, Franks HA, Televantos C, et al. Impaired circulating myeloid CD1c+ dendritic cell function in human glioblastoma is restored by p38 inhibition - implications for the next generation of DC vaccines. *Oncoimmunology.* 2019;8:1593803. DOI PubMed PMC
74. van der Vos KE, Abels ER, Zhang X, et al. Directly visualized glioblastoma-derived extracellular vesicles transfer RNA to microglia/macrophages in the brain. *Neuro Oncol.* 2016;18:58-69. DOI PubMed PMC
75. Zhang L, Yang J, Zhou Z, et al. A zinc transporter drives glioblastoma progression via extracellular vesicles-reprogrammed microglial plasticity. *Proc Natl Acad Sci U S A.* 2025;122:e2427073122. DOI PubMed PMC
76. Madhu LN, Kodali M, Rao S, et al. Intranasal human NSC-derived EVs therapy can restrain inflammatory microglial transcriptome, and NLRP3 and cGAS-STING signalling, in aged hippocampus. *J Extracell Vesicles.* 2026;15:e70232. DOI PubMed PMC
77. Manni G, Gargaro M, Ricciuti D, et al. Amniotic fluid stem cell-derived extracellular vesicles educate type 2 conventional dendritic cells to rescue autoimmune disorders in a multiple sclerosis mouse model. *J Extracell Vesicles.* 2024;13:e12446. DOI PubMed PMC
78. Mulcahy LA, Pink RC, Carter DR. Routes and mechanisms of extracellular vesicle uptake. *J Extracell Vesicles.* 2014;3:24641. DOI PubMed PMC
79. Kim DO, Nguyen QT, Choi YC, et al. Strain- and species-specific immune responses to human adipose stem cell-derived extracellular vesicles: a comparative pharmacological evaluation in mice and human PBMCs. *Eur J Pharm Biopharm.* 2026;222:115008. DOI PubMed

Disclaimer/Publisher's Note: All statements, opinions, and data contained in this publication are solely those of the individual author(s) and contributor(s) and do not necessarily reflect those of OAE and/or the editor(s). OAE and/or the editor(s) disclaim any responsibility for harm to persons or property resulting from the use of any ideas, methods, instructions, or products mentioned in the content.

© The Author(s) 2026. Open Access This article is licensed under a Creative Commons Attribution 4.0 International License (https://creativecommons.org/licenses/by/4.0/), which permits unrestricted use, sharing, adaptation, distribution and reproduction in any medium or format, for any purpose, even commercially, as long as you give appropriate credit to the original author(s) and the source, provide a link to the Creative Commons license, and indicate if changes were made.